Applying Dynamic Damping to Robotic Vitreoretinal Surgery

L.M. Kranendonk

Technische Universiteit Delft

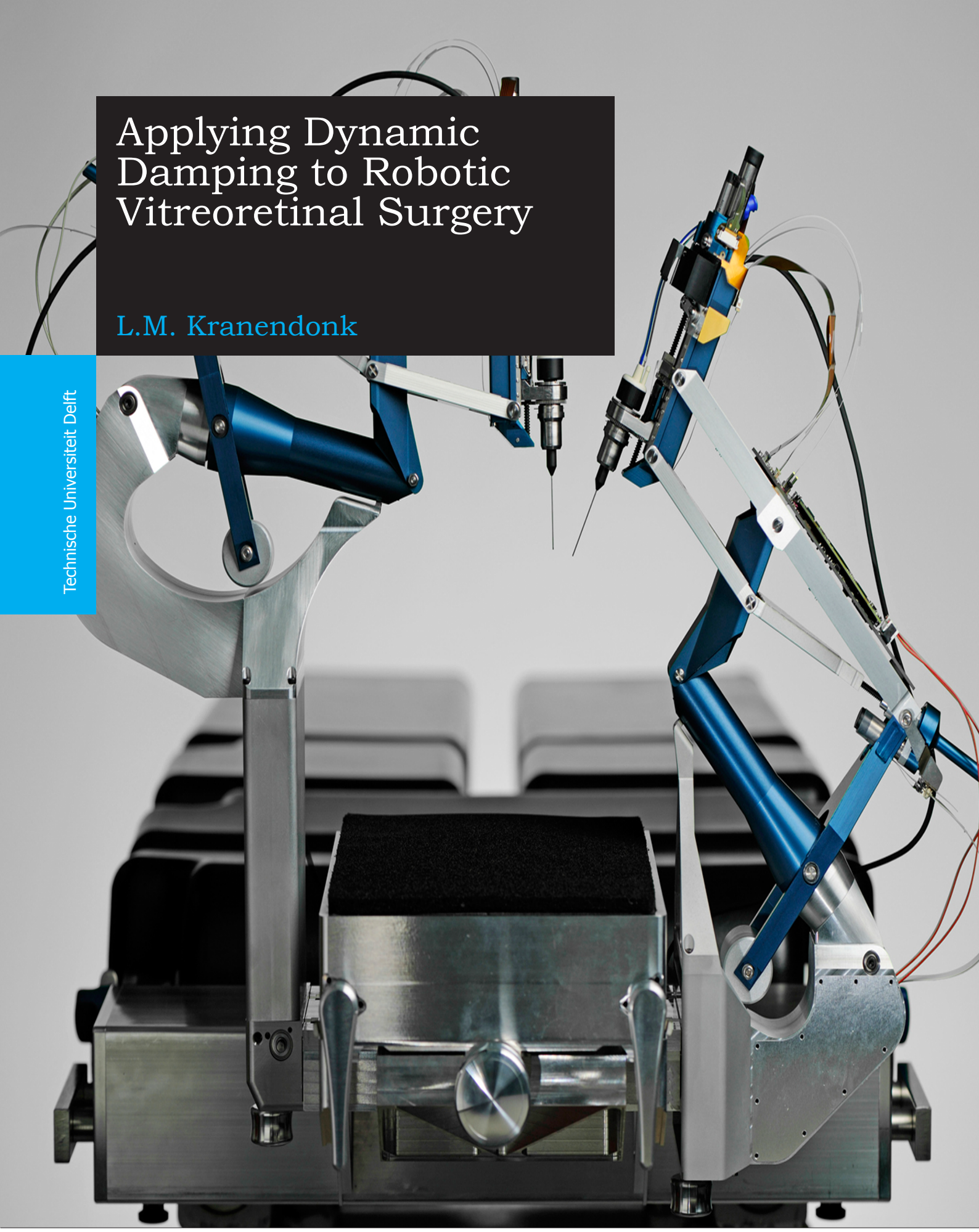

TU Delft Delft University of Technology

Challenge the future

Applying Dynamic Damping to Robotic Vitreoretinal Surgery

by

L.M. Kranendonk

to obtain the degree of Master of Science
at the Delft University of Technology,
to be defended publicly on Thursday October 12, 2017 at 1:00 PM

Student number:	4016173	
Project duration:	February 2017 – October 2017	
Thesis committee:	dr. ir. D. Abbink,	TU Delft, supervisor
	Dr. J. J. van den Dobbelsteen,	TU Delft
	ir. S. M. Petermeijer,	TU Delft
	ir. Y. G. M. Douven,	PRECEYES B.V.

This thesis is confidential and cannot be made public until October 12, 2020

TU Delft

Acknowledgement

First of all I would like to thank my supervisor David Abbink. His enthusiasm in his courses and lectures drew me towards this field of research. David was able to motivate me when I was down, but also made me think twice when I was moving too fast. David is a very social person, and he has gathered a group of very friendly and motivated people around him in the Haptics Lab. I should not forget to mention Tricia Gibo, as she was my daily supervisor in the beginning of the project. It was a great loss for both me and the university when Tricia moved on to new opportunities.

As mentioned above, the Haptics Lab was a very kind environment to spend my last months at the TU Delft. Although I had a good time with everyone, I should mention a few names. Timo Melman helped me wrestle through the ins and outs regarding the statistics and Bastiaan Petermeijer kindly offered to review my report.

I should also mention the people from PRECEYES B.V., Maarten Beelen and Yanick Douven. Your critical questions during our Skype meetings helped me keep on track, and although they sometimes made me a bit nervous, they were always very beneficial. Of course I would also like to thank my parents, who both supported me each in their own way.

Laurens Kranendonk
Delft, October 2017

Contents

List of Abbreviations

ANOVA	Analysis Of Variance
DOF	Degree Of Freedom
ERM	Epiretinal Membrane
FS	Force Scaling
IM	Instrument Manipulator
MC	Motion Controller
OCT	Optical Coherence Tomography
OR	Operating Room
PV	Proportional Velocity
PVL	Proportional Velocity Limit
RAMIS	Robotic Assisted Minimally Invasive Surgery

List of Figures

List of Tables

Abstract

Vitreoretinal surgery remains one of the most challenging types of surgery due to the delicate nature of the eye, the minimally invasive nature of the procedure, the small operating space and lack of depth perception. One of the procedures that is performed during vitreoretinal surgery is Epiretinal Membrane (ERM) Peeling , during which the surgeon has to peel a membrane of the retina without damaging the retina. Robotic membrane peeling can greatly improve clinical outcome because of increased accuracy, tremor reduction and little to no fatigue effects. However, depth perception still remains a problem, because the surgeon is looking at the procedure from directly above through a microscope, therefore creating a 2-D vision. The topic of this study is a tele-operated robotic system that is specialized in vitreoretinal surgery. The PRECEYES surgical system is equiped with an OCT distance sensor that can estimate how far away the tip is from the retina, but not accurately enough for traditional 'forbidden region' assistance. This study aims to design and evaluate a proof-of-concept for haptic support during robot-assisted vitreoretinal surgery, by means of an artificial damping-field on the master device. The main contributions of this study were 1) to create a simulation environment for robot-assisted vitreoretinal surgery; 2) to design and implement a damping field on this simulator; and 3) to perform a human-in-the-loop experiment to compare unassisted control behaviour to assisted control behaviour

To study the effect of the damping field, a simulation of the procedure was created. A physical haptic master device controls a virtual slave in a simulated environment. The participants (n=16) were asked to move the instrument towards the retina, and then gently move it through a ring on the surface of the retina. This task forced the participant to make a peeling motion that is typical for ERM peeling. The experiment had 4 conditions: a small or a large target, with the damping field switched on or off. Each of the 16 participants had to perform 10 successful runs per condition. A retina puncture resulted in a failure and is not counted as a successful run. Results showed that for the small target, the average number of punctures per participant decreased from 2.4 to 0.9 when the damping field was enabled. The average completion time was comparable for both small target conditions, and likewise for the large target conditions. It was observed that participants decreased their velocity at the same distance of the retina for multiple runs when the damping field was active, which indicates that the participants were able to estimate the distance to the retina using the damping field. Furthermore, the damping field enabled the participants to employ a larger safety margin (distance between the instrument and the retina) between the instrument and the retina.For the experimental conditions studied, the designed damping field decreased the amount of punctures without affecting the task completion time. Improvements to the damping field, such as an exponential increase of the damping coefficient and moving the starting point closer to the retina could increase the performance of the system.

1 Introduction

Robot-Assisted Minimally Invasive Surgery (RAMIS) is a fast-developing field that has already yielded successful clinical applications. RAMIS combines the advantages of both minimally invasive surgery and robotic surgery. Minimally invasive surgery leads to less recovery time, less scar tissue and a reduced time in the hospital for the patient. Robotic surgery potentially increases the accuracy and precision of the surgeon's motion, and in delicate procedures this can lead to a better clinical outcome.

Because of its delicate nature, vitreoretinal surgery can benefit a lot from Robot-Assisted Minimally Invasive Surgery. All procedures that take place inside the eye or at the surface of the retina are defined as vitreoretinal procedures. Vitreoretinal surgery requires extreme accuracy and precision because of a number of reason. First of all the organ itself is very small; the diameter of the average eye is 25 mm [29]. Vitreoretinal procedures have to take place within this space. Secondly, vitreoretinal surgery is almost by definition minimally invasive, since it is not possible to cut open the eye. Furthermore, the anatomy of the eye is very delicate. When performing procedures on the retina one has to be extremely careful, since the retina has a thickness of only 60 μm [28].
Another complicating factor is that the surgeon has a 2-D vision of the procedure, since he is looking through a microscope that is looking through the lens of the eye.
PRECEYES B.V. has developed a robotic surgical system that is designed specifically for vitreoretinal procedures. At the moment the company is focusing on ERM peeling, one of the procedures that is executed during vitreoretinal surgery. Their system is equipped with an OCT-distance sensor and they are looking for a way to use this sensor information to increase the performance of the surgeon. This study aims to find a way to intuitively feedback this information to the surgeon.
Haptic stimuli are one way to feedback this information, and when applied in the right way, haptic stimuli can be more intuitive than visual or auditory feedback. Because inaccuracy of the instrument position is inherent to this problem, a haptic interface that is redundant for errors was chosen: a dynamic damping field that increases as the instrument moves closer to the retina. This leads to the following research question:

Can a dynamic damping field based on instrument position increase safety during robotic vitreoretinal surgery?

Chapter 2 serves to familiarize the reader with the terminology and difficulties of robotic vitreoretinal surgery. In Chapter 3 the design of the simulation environment, the experimental design and damping field design are discussed. The results of the experiment are given in Chapter 4. In Chapter 5 the results are discussed, after which a conclusion is given in Chapter 6

2

Background

This chapter serves to get the reader up to speed with the terminology and procedures at hand. In Section 2.1 the basics of vitreoretinal surgery and especially Epiretinal Membrane Peeling are discussed. In Section 2.2 the details of the PRECEYES Surgical System are discussed, the robot that is topic of this research. In Section 2.4 the application of haptic guidance in surgical settings are analyzed. Parts of this chapter are taken from the literature study of the author [16].

2.1. Vitreoretinal Surgery

Vitreoretinal surgery embodies all procedures performed at the inside surface of the eye and the retina. It is used for various types of conditions such as retinal detachment, macular holes, vitreous bleeding and Epiretinal Membrane (ERM) peeling. vitreoretinal surgery is performed by a vitreoretinal specialist. Vitreoretinal surgery is an additional specialization to ophthalmology (ophthalmology deals with the physiology and diseases of the eyeball in general). A schematic image of a vitreoretinal procedure is given in Figure 2.1 A lot of different procedures are performed during vitreoretinal surgery, but the general approach remains

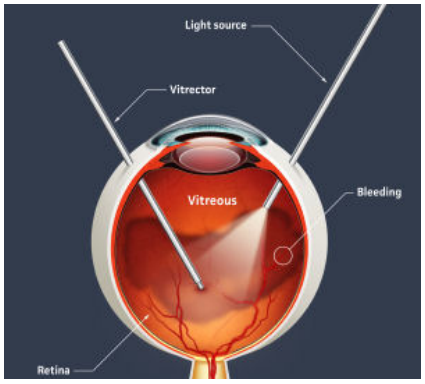

Figure 2.1: Visual representation of a typical vitreoretinal surgery. The vitrector is used to remove the vitreous fluid

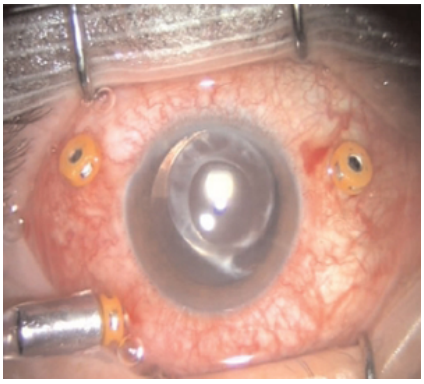

Figure 2.2: Placement of the three trocars for instrument insertion. The vitrector can be seen in the down-left corner

the same [21]. First off the patient is put under a full anaesthesia. This will greatly reduce eye motion during the procedure and will limit discomfort to the patient. Sometimes the procedure is performed under a local anaesthesia, but only if the patient's condition does not allow for a full anaesthesia.

When the patient is fully anesthetized, a clamp is placed to keep the eyelids open and prevent the eye from moving. After this the eye is thoroughly sterilized using an iodine solution. When the eye is completely sterile, the surgeon places the first trocar right next to the cornea through the pars-plana. An infusion is placed in this trocar which removes the vitreous humor and replaces it with a saline solution. This procedure is called *pars plana vitrectomy* since the entry-point is through the pars plana and the vitreous humour is removed (vitreous + ectomy (removal) = vitrectomy).

The surgeon places another two trocars opposite of each other. One of the trocars is used to insert a light source, the other one is used to insert a tool. 2.2 shows the three trocars in place with the infusion. Because the trocars are in place, the surgeon is able to switch instruments without having to make another incision.

The surgeon has a selection of tools available, depending on the procedure to be performed. Among others he can use a small gripper and a laser. During the procedure the eye is regularly flushed with sterilized water to remove blood. At the same time a protective gel is sprayed on the cornea to prevent it from drying out and getting damaged.

A wide-scope microscope is brought very close to the eye so the surgeon can see the inside of the eye through the pupil. If necessary, the pupil can be widened using small hooks to further enhance visibility. After the procedure is completed, the trocars are removed. In some cases the layers of the sclera and chloroid fold over each other closing the gap that the trocar left. If this is not the case, stitches are required to seal the incision.

2.1.1. Epiretinal Membrane Peeling

An Epiretinal Membrane (ERM) is a thin layer that forms on top of the retina in response to changes in the vitreous humor. This membrane can impair the vision of the patient since it is blocking the retina. Age plays a role in the pathology of ERM since the mean age of ERM diagnosis is 65 years [10]. Peeling of this membrane can restore vision and studies show that removal of the ERM does not only restore vision but also decreases the odds of recurrence [2].

The membrane can be removed by means of vitreoretinal surgery. First off, colored marker fluid is injected in the vitreous which colors the ERM. Alternatively, a marker can be used which colors everything but the ERM. The surgeon 'peels' the delicate membrane off the retina. This delicate task requires a lot of precision and concentration from the surgeon.

The thickness of the membrane is on average about 60 μm [28], so it is very hard to manipulate.

The surgeon first peels of a little edge which he can grab, and then makes slow circular motions to reduce the tension and remove the membrane. All this has to be done very carefully, since the thin membrane has to be picked of the retina without touching the retina. A puncture of the retina could lead to permanent damage to the patient's vision.

Patients that underwent ERM peeling surgery gain about two lines of visibility on the Snellen-chart [29], which is the well-known poster with letters depicted in 2.3.

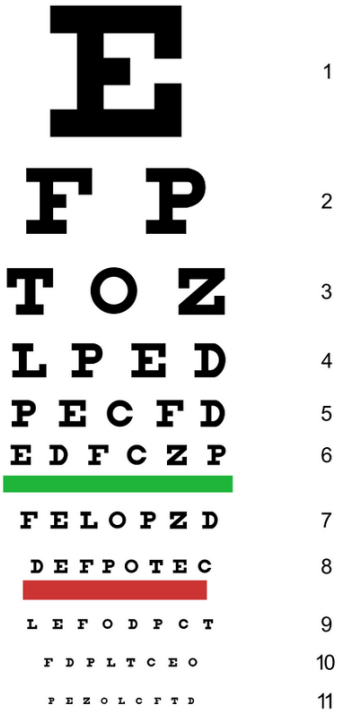

Figure 2.3: Snellen chart

2.1.2. Vitreoretinal surgery challenges and difficulties

Vitreoretinal surgery is regarded as one of the most difficult procedures performed on the eye. The space to maneuver is extremely small: the diameter of the entire eye is about 25 mm and the surgeon has to perform the operation within this space. Furthermore, the tools go in the eye through small incisions in the sclera which means they have to pivot around these entry-points without stressing the sclera too much. Due to the delicate structures, the surgeons have to deal with forces that are lower than their sensory threshold. This means that the surgeon is mainly relying on his visual senses. The procedures performed are on a microscopic scale, especially the manipulations performed within the eye. A precision in the scale of micrometers is required for some manipulations. One can imagine that the natural tremor that every surgeon has to some degree can severely influence the result of the operation. Furthermore, the visibility is very limited. The major factors are summarized below:

Microscopic forces During vitreoretinal procedures the surgeon encounters microscopic forces that are below the sensory threshold. A two-fold study by Gupta et al. [11] determined that the sensory threshold for surgeons during vitreoretinal surgery is 7.5 mN, and that roughly 80% of the encountered forces during vitreoretinal surgery are below this threshold. Not only are the forces dealt with incredibly small, but they are also fed back to the surgeon through the instrument. The instrument also experiences reaction forces from the trocar which it pivots around, and these forces are much larger than the forces at the

tool-tip. One can imagine that it becomes impossible to sense the forces at the tool-tip with so much noise. The membrane that is peeled of the retina is only 60 μm. This means that the reaction forces during peeling are basically zero, and the surgeon heavily relies on his vision to perform this operation.

Physiologic Tremor All individuals experience a certain natural tremor. This natural (physiologic) tremor manifests itself at a frequency between 8 and 12 Hz [9]. The severity and frequency of this tremor vary from person to person. For surgeons operating on such a small scale this tremor plays an important role. Physiologic tremor is in the order of 100 μm when translated to the tip of a vitreoretinal instrument [17]. The surgeon deploys techniques to limit this tremor to a minimum. The study in [9] has recognized different factors that influence the tremor. Factors that worsen the tremor are caffeine, sleep deprivation, fatigue and long operations times. Resting the wrist on a surface will decrease the tremor and this is employed by vitreoretinal surgeons.

Minimally Invasive Surgery Vitreoretinal surgery has a lot in common with general Minimally Invasive or 'keyhole' Surgery. The instruments enter the body through small incisions and the operation has to be performed in a small confined space. The instruments 'pivot' around the entry-point, which means their control is inverted and different from normal surgery. The diameter of the entire eye is 25 mm, and all procedures have to be performed within this space on even smaller structures. Since the instruments travel through small incisions, their control is inverted. It takes additional training and time for the surgeon too get used to this effect.

Delicate structures Every part of the eye is of a very delicate and sensitive nature. From the cornea to the retina, everything is prone to irreversible damage. The instruments enter the eye through trocars in the sclera. Because the instruments pivot around the trocars, they put a force on the sclera. The surgeon has to make sure that the forces exerted do not damage the sclera. In retinal detachment, the surgeon has to handle the detached retina which is between 0.1 and 0.33 mm thin.

Patient Motion During vitreoretinal surgery the patient still exerts some motion, despite receiving a full anaesthesia. Causes of this motion are breathing, beating of the heart and pulsation of blood through the veins. Although the motions are very small, they still have to be taken into account when performing difficult tasks such as membrane peeling or vein cannulation. During membrane peeling the retina can move due to blood pulsing through the veins. Vein cannulation is even harder, since the vein sometimes has to stay cannulated for 20 minutes while it is pulsing.

Depth Perception The surgeon is looking at the procedure through the lens of the eye. The view is enhanced by a microscope, but because the vantage point is placed directly above the eye, a 2-D vision is created which makes it very difficult to estimate depth. Figure 2.4 illustrates this.

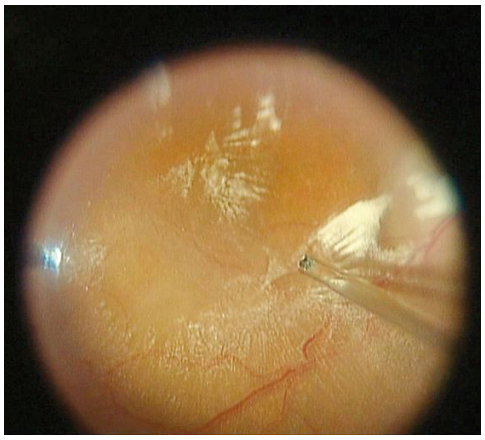

Figure 2.4: Typical view of the surgeon during vitreoretinal surgery

2.2. PRECEYES Surgical System

The PRECEYES Surgical System is a robotic tele-operated surgical device developed by PRECEYES BV, designed to assist surgeons during vitreoretinal surgery. The device enhances surgical precision and fits in the current surgical workflow. The system is a hybrid system, since the surgeon is controlling the device with one hand while operating a manual instrument with the other hand. The system consists of an Instrument Manipulator (IM) holding and moving the instrument as commanded by the surgeon by hand through the Motion Controller (MC).

The instrument connected to the manipulator enters the eye through a trocar, just like in manual surgery. The instrument manipulator is in designed in such a way that the instruments always rotates around the entry-point. This Remote Center of Motion is a mechanical property of the system to ensure no motion takes place at this point. The RCM still needs to be placed at the point of entry though. This is achieved by connecting the instrument to the trocar with a trocar connector. Not only does this ensure that the RCM is placed at the trocar entry, but it also fixates the eye. The Motion Controller is designed with a button. When

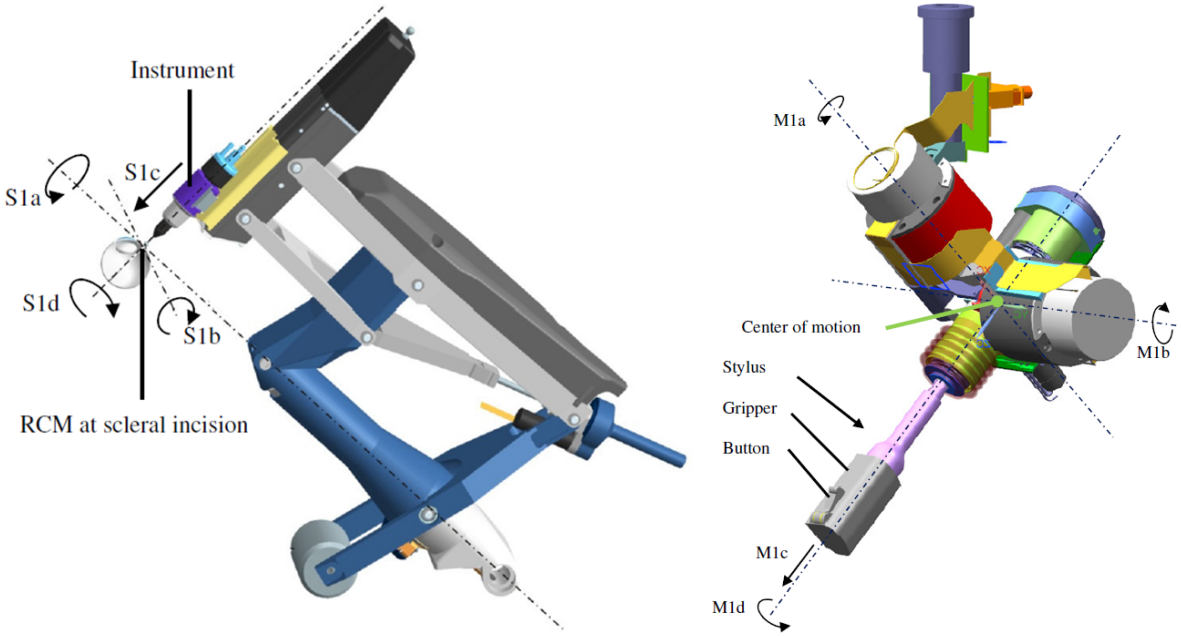

Figure 2.5: The Instrument Manipulator (left) and Motion Controller ©PRECEYES BV

the button is pushed the Instrument Manipulator follows the motion of the surgeon, but when the button is released the Instrument Manipulator will remain in a fixed position. This allows the surgeon to always move the Motion Controller in a comfortable position. Furthermore, when a joint limit of the Motion Controller is reached before the limit of the Instrument Manipulator is reached, the Motion Controller can be moved back into neutral position in order to allow manipulation in all directions.
The Instrument Manipulator is mounted on a cantilever system which enables the surgeon to quickly move the instrument towards or away from the patient. In case of a clinical emergency the instrument can be moved away, but also when the surgeon decides to do (part of) the procedure manually.
The PRECEYES Surgical System has some clear advances over conventional vitreoretinal surgery. Due to the separate master and slave it is possible to implement some assistive control algorithms. One that is already implemented is tremor reduction. The system filters out the natural tremor that the surgeon imposes on the Motion Controller. This increases the precision and decreases the number of undesirable motions that could possibly harm the patient. Another option that the surgeon has is the level of motion scaling. For accurate tasks, the surgeon can decrease the motion scaling between the master and the slave. He then has to move the master over a large distance in order to move the slave over a smaller distance, therefore increasing precision. More control algorithm such as damping can be applied to the system, and the surgeon is able to switch between the different modes using the touch screen.

2.2.1. OR Setup

An overview of the PRECEYES surgical system in an Operating Room (OR) setting is given in Figure 2.6. It can be seen that the Instrument Manipulator is connected to the headrest. The patient's head is also connected to the headrest, which means that the position of the Instrument Manipulator relative to the patient's head will not change in case of motion of the patient's head or headrest. On the right side the Motion Controller that the surgeon uses to move the Instrument Manipulator can be seen. The touch-screen enables the surgeon to switch between different control modes. The surgeon looks into the eye through the microscope, and is able to adjust the level of zoom with the foot pedal. The vitrectomy foot pedal regulates the suction power used for the vitrectomy. The microscope and both foot pedals are equivalent to the hardware used during conventional vitreoretinal surgery.

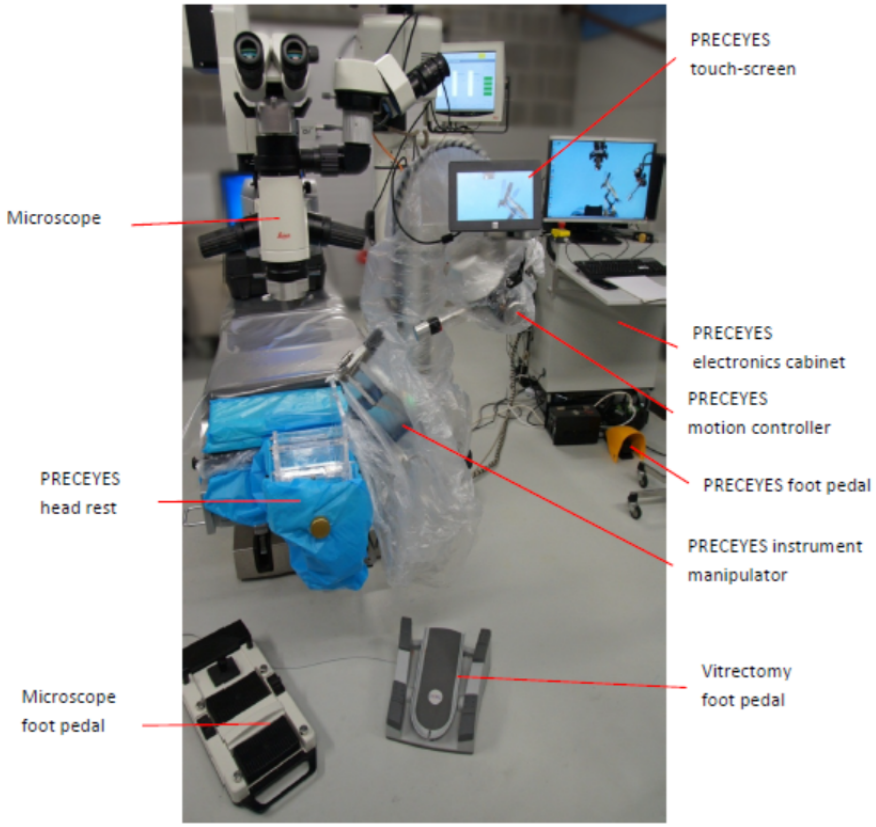

Figure 2.6: The PRECEYES Surgical System in a clinical setting

2.2.2. OCT Sensor

The Instrument Manipulator of the PRECEYES Surgical System is equipped with an Optical Coherence Tomography (OCT) sensor. This sensor uses light to image (partly) opaque materials. The retina is very suitable for OCT sensors, since the biological material has the right reflective properties. The sensor measures in one direction (along the axis of the instrument) and is able to measure different layers. Therefore it is possible to measure the distance to the retina and the underlying layers along one axis. Samplonius et al. studied the OCT-sensor that is used by the PRECEYES Surgical System and published the results in [24]. The accuracy of the retina position estimation stayed within 40 μm for 99% of the time. The OCT-sensor can be used to provide the surgeon with more information about the position of the instrument. Because the surgeon has a 2-D, enlarged view of the surgical area it is very hard to perceive depth. The sensor can estimate the position of the instrument relative to the retina, which is valuable information for the surgeon. The sensor has a maximum operating range of 3 mm, at larger distances the sensor becomes too inaccurate.

2.3. Natural Force Feedback

When dealing with tele-operated robotic systems, it is easy to think of the advantages: robots can exert more force, have a wider range of motion and can be designed specifically for one task. However, a downside of robotic systems is the loss of touch. One of the most important touch (haptic) senses is force feedback. When a human peels an egg, he uses his senses to estimate how much force he can apply. Robotic systems can be equipped with force feedback as well. In order to do so, the force exerted by the object must be measured in some way. This force is then converted in a force on the controller. The person controlling the system can then 'feel' the robotic arm colliding with objects.
The Da Vinci Surgical System is one of the most well-known surgical robotic systems. The system is not equipped with force feedback. Although many studies indicate that the system could benefit from force feedback (an overview is given in[19]), it has not been integrated with the system. This is probably due to an economic trade-off. In order to apply force feedback the system would need a master device that is actuated in all DOF's, and a slave that can measure forces in all directions (accurate enough). The Da Vinci Surgical System is designed for minimally invasive surgery, meaning the force sensors have to be small enough (i.e. expensive) to be integrated with the instruments. Last but not least, licensing in the medical field is very expensive, and a system equipped with force feedback would have to be licensed all over again. The PRECEYES Surgical System had Force Feedback or perhaps even haptic assistance in their mind when they were designing the system, as their system has actuated joints in the Instrument Manipulator. Although the possibility is there, right now no force feedback is applied in the system.
Wagner et al. [26] did a comparative study for a blunt dissection task between a system with and without force feedback and came to the conclusion that force feedback leads to more accurate performance and less tissue damage. In [15] a dissertation is done assessing tissue handling skills during minimally invasive surgery when force measurements are fed back visually.

2.4. Haptic Assistance

In a world where more and more tasks are executed automatically, Shared Control has a slightly different view on automation. Of course there are a lot of tasks that are extremely suitable for automation. Think of the assembly line in a factory, where the same task is executed over and over again. Or the cruise control in an average car. What these tasks have in common is that they are very repetitive and unexpected events rarely or never occur, which make them suitable for automation. When tasks become more diverse and varying, the performance of automation declines. These kind of tasks could benefit from Haptic Shared Control. In Figure

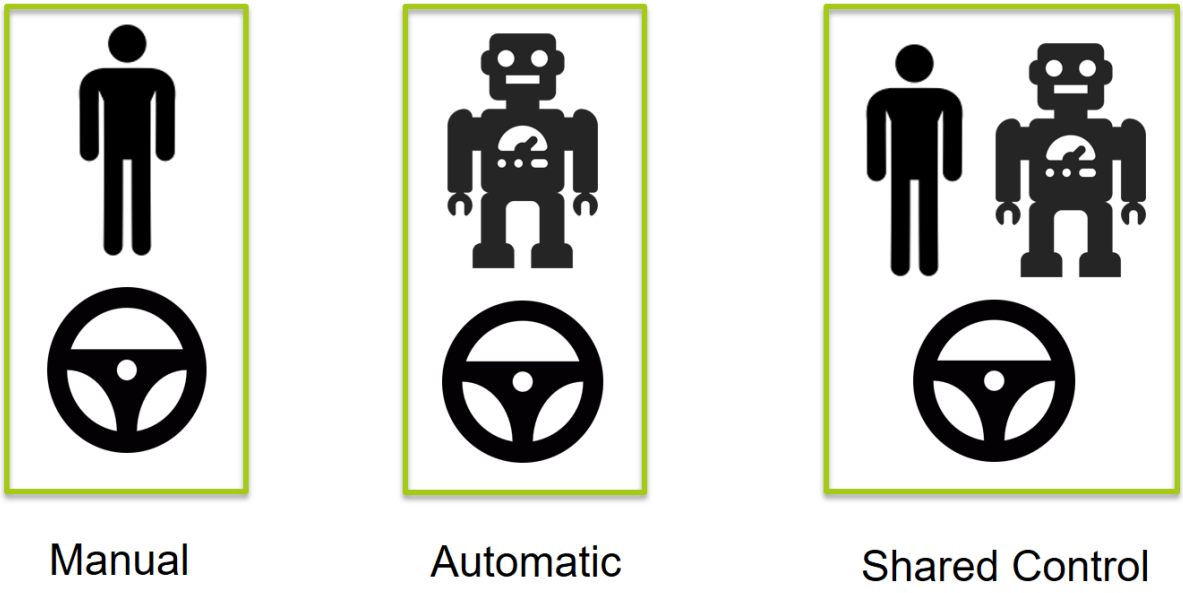

Figure 2.7: The three paradigms: Manual, Automatic and Shared Control

2.7 a schematic drawing of the three control paradigms are given. To illustrate an example of Shared Control a car driving task is taken. At first there's the manual driving task. The driver controls the car manually and no

automation is applied. The driver is able to anticipate to unexpected circumstances such as a person crossing the road or a light suddenly turning to red. However, he might lose his attention or even fall asleep when the driving task is executed for a longer amount of time. A solution for this problem could be to fully automate the driving task, depicted in the middle figure. The driving task could be performed fully automated. Indeed, the first autonomously driving cars are being developed right now. As it turns out, they perform very well in the repetitive, 'standard' driving task. But to be able to adapt to unexpected events, these systems require an incredible amount of training data in which virtually every situation has occurred. Shared Control is a paradigm that fits between 'Manual' and 'Automated' and aims to combine the best of both worlds. In a Shared Control environment, both the operator and the controller collaborate in order to perform a certain task. There are various systems that assist in car-driving tasks that are based on this principle. For example the Lane Keeping Assist, which helps the driver to steer within the driving lane. When the driver sways from the middle, assistive torques are exerted on the steering wheel which keeps the car in the middle. When the car is in the middle, no torques are exerted. Therefore the system is only active when needed. In this example the assistive torques are exerted through the steering wheel, the input device. This is called *Haptic Shared Control*, because the interaction occurs through the sense of touch. Other forms of interaction are auditory feedback (parking sensors) or visual feedback (speedometer).

2.4.1. Haptic Assistance in a surgical setting

In this section an overview of the application of Haptic assistance in a clinical setting is given. The applications are ordered by the type of assistance that is given.

Medical application of forbidden-region virtual fixtures

There are several ways to provide the user with haptic feedback. Which one is optimal is dependent on the task performed. Forbidden region virtual fixtures are virtual walls generated through software that stop the instrument from moving in sensitive areas that could be damaged by the end-effector. The regions where the end-effector cannot go are called 'forbidden regions'. When the user wants to move the slave into a forbidden region, the haptic software will increase stiffness in that direction as if the user was bumping into a wall. The concept of virtual fixtures was introduced by Rosenberg [23]. Bettini et al. [6] applied forbidden-region virtual fixtures for positioning and curve-following tasks. In all tasks the assisted execution outperforms unassisted execution in terms of position accuracy and completion time.
Forbidden-region virtual fixtures can contribute to medical applications. Park et al. applied to forbidden-region virtual fixtures to robotic catheter navigation [20]. The virtual fixtures prevented tissue perforation by the catheter. Yamamoto *et al.* [30] have developed an experimental medical application tested on artificial tissue which proved to be successful. They determined pre-operatively what the forbidden regions would be and implemented this in a visual and haptic overlay. However, this was a static application whereas many operations take place in a moving and dynamic environment. Ren et al. developed dynamic virtual fixtures for minimally invasive beating heart surgeries using potential fields [22]. When applying virtual fixtures one has to make a trade-off between freedom of movement and performance. If you apply hard boundaries which cannot be passed, you ensure that the instrument does not move into the forbidden region. On the other hand, if unexpected circumstances require the surgeon to move into the forbidden region, he cannot do so. Therefore one could argue to apply more compliant boundaries, with the risk of unwanted trespassing of the forbidden regions as a consequence. A balance between these two arguments must be found and is dependent on the task performed.

Medical Application of Attractive virtual fixtures Attractive virtual fixtures are opposite to forbidden-region virtual fixtures. These virtual fixtures provide guiding forces that assist the user to execute a predetermined task. A requirement to apply attractive virtual fixtures is that the optimal path or task performance is pre-defined. For robotic surgery this can be for instance the circumference of a tumor that is removed. The position of the tumor can be determined pre-operatively and the virtual fixtures can aid to follow the predefined path to cut away the tumor. In [18] a design is proposed to use attractive virtual fixtures during training. In [25] shared control is applied to a needle steering task.

2.4.2. Assistive technologies in vitreoretinal surgery

Due to the microscopic force and visual sensors being developed, more information has become available to the vitreoretinal surgeon. This data can simply be displayed on a monitor, but researchers are looking into

other ways to feed back this information to the surgeon. Based on this sensory data, guidance virtual fixtures can assist the surgeon in manipulating the right places and forbidden region virtual fixtures can help prevent damage to the retina, optic nerve or sclera.

Feedback of force sensors in vitreoretinal surgery
Current force sensors are accurate and small enough to be used during vitreoretinal surgery. In [4] a prototype is suggested using the EyeRobot2 (the latest version of the Steady-hand Eye Robot). In this paper a set-up is proposed that adds the master manipulator device of the DaVinci Surgical System in order to tele-operate the EyeRobot2. This enables the researchers to apply active bi-lateral virtual fixtures to the system. This is only a theoretical design, and the EyeRobot2 is not designed to be tele-operated. It does not have enough actuated joints to perform all motions and therefore this set-up seems to be a bit of a work-around.

The same authors have developed a an experimental set-up for the Steady-Hand Eye Robot with integrated microscopic force sensors [3]. Based on these measured forces they applied a number of feedback methods: Proportional Velocity Control, Linear Force Scaling Control, and Proportional Velocity Control with Limits. The aim of this research was to provide assistance for Epiretinal Membrane Peeling (see 2.1.1) by minimizing the reaction forces. Each of these control methods will be discussed below.

Proportional Velocity Control (PV)
This control method regulates the velocity at the tool tip and makes it proportional to the forces applied to the handle. The scaling factor a is chosen in such a way that 1 N of force on the handle equals 1 mm/s tool velocity. This control method is written out in 2.1. F_h is the applied force on the handle.

$$\dot{x} = aF_h \tag{2.1}$$

Linear Force Scaling Control (FS)
This control method amplifies the measured tool tip forces to be proportional to the handle forces. This proportionality is tuned in such a way that the measured tip forces in the range of 0-10 mN map to handle forces in the range of 0-5 N. The control method is designed in such a way that the user has to apply a larger force in the direction where tool tip forces are measured in order to move the instrument. To the user this will feel like he can feel the tip forces. This control method is written out in 2.2. γ is the scaling factor that maps the measured tool tip forces proportionally to the handle forces. It was determined to be 500. F_t is the measured tool tip force. Note that the reaction tool tip force is inversely proportional to the handle force, therefore they are added to each other in the formula. This will in fact require the user to apply more force in the opposite direction of the reaction force, effectively giving the user the sensation of sensing the microscopic reaction forces.

$$\dot{x} = F_h + \gamma F_t \tag{2.2}$$

Proportional Velocity Limit (PVL)
This control method puts a limit on the maximum velocity of the tool tip dependent on the measured tip forces. When reaction forces are high, the maximum velocity is decreased. When the reaction forces are low, the maximum velocity is increased. Below a certain threshold of reaction force f_1 (empirically found to be 1 mN) no velocity limit is valid and the Proportional Velocity Control is applied. Similarly, above 7.5 mN of reaction forces a fixed velocity limit of $v_2 = 0.1mm/s$ is applied. The velocity limit as function of the reaction force is given in 2.8.

Auditory feedback
All three control methods have been tested with and without auditory feedback. This auditory feedback functions like a parking sensor, where the frequency of the beeps is lower for low reaction forces, and higher for high reaction forces. The auditory feedback profile is given in 2.8.

The three proposed control methods have all been evaluated with and without auditory feedback, and for comparison a test is done without any control method (Freehand). The results are given in 2.9[h!]. As can be seen, the Force Scaling and Velocity Limiting methods yield the best results. The authors conclude that Force Scaling is the best method since it yields the lowest tip forces on average, but it has a longer completion time. One could argue that Velocity Limiting is the best methods since it has a shorter completion time and only slightly higher tip forces. Velocity Limiting does not benefit from auditory feedback, in contrast with the other experiments.

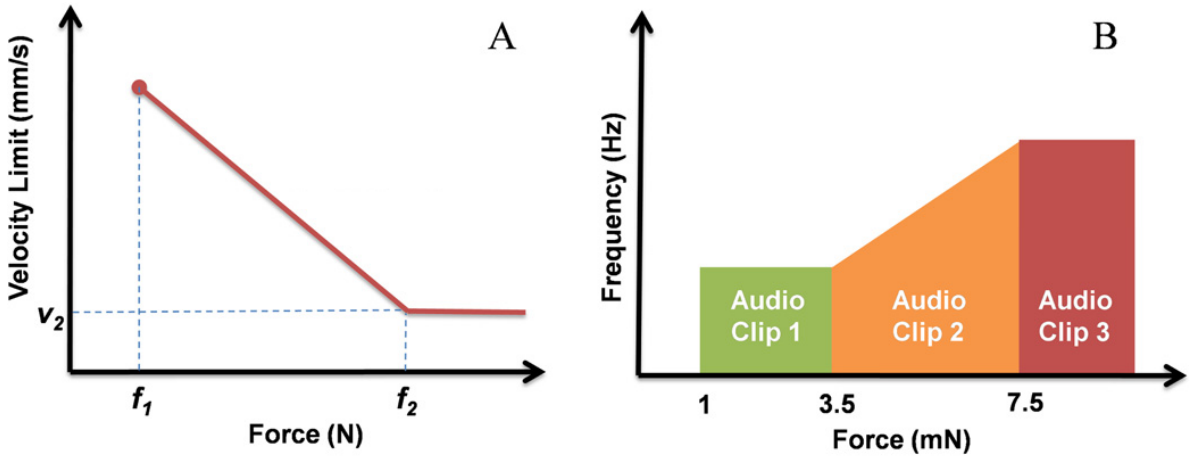

Figure 2.8: A) Velocity limit for PVL B) Auditory feedback profile [3]

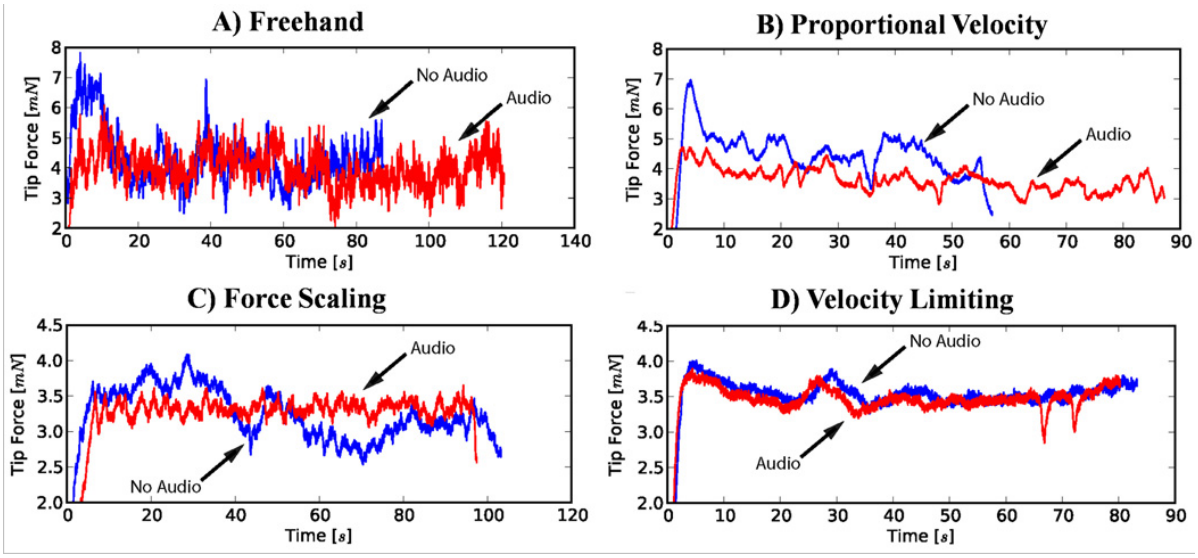

Figure 2.9: Plots of the different control methods, with and without auditory feedback

A follow-up study presented in [12] and [13] has been performed which added two extra force sensors to measure the forces on the sclera (where the instrument enters the eye through the trocar). Similar control methods were successfully applied to minimize the forces on the sclera.

Feedback of visual sensors in vitreoretinal surgery

The information collected by visual sensors is of great value and can be fed back to the surgeon in several ways. Dewan et al. performed a proof-of-concept study to construct forbidden region virtual fixtures based on visual sensors [8]. This is still a very crude proof-of-concept since the visual sensor is located externally from the manipulation device, but it shows that virtual fixtures can be generated based on visual data. Becker et al. utilized the Micron handheld device and external camera's to create position based virtual fixtures [5]. The authors used visual data to provide assistance during membrane peeling, where other researchers implemented force sensors. They implemented a virtual wall based on visual data to prevent the instrument from puncturing the retina and motion scaling and tremor reduction to increase precision. They tested their set-up on a phantom retina consisting of a thin plastic wrap stretched on top of a rubber slide. They reduced the exerted forces by 40 to 70 %. In [31] the authors have integrated an OCT sensor in the forceps used for membrane peeling. The OCT data is displayed as a side-view, showing the distance of the instrument to the surface. The authors used both a manual controlled forceps and a tele-operated one and concluded that tele-operated surgery with tremor reduction, motion scaling and OCT feedback yielded the best results.

3

Materials & Methods

This chapter will describe the models, software and hardware used to obtain the experimental results. In Section 3.1 the design of the simulation environment is elaborated. The set-up of the experiment is explained in Section 3.2, after which the designs for haptic assistance will be treated in Section 3.3

3.1. Simulation Design

3.1.1. Model Architecture

The model architecture that is used for the simulation is given in Figure 3.1. The human (in this case the surgeon) exerts control torques on the master device in order to perform the task at hand. Two flows of information can be identified: from left to right and from right to left. The flow from left to right is the human interacting with the master device. The position of the master device is converted into a (simulated) slave position, which is fed to the simulated environment. The second flow of information is going from right to left: Based on the simulated environment a visualization is created that is fed back to the operator. Based on the slave position combined with the simulated environment, the Guidance Controller generates assistive torques that are fed back to the operator by the Master Device.

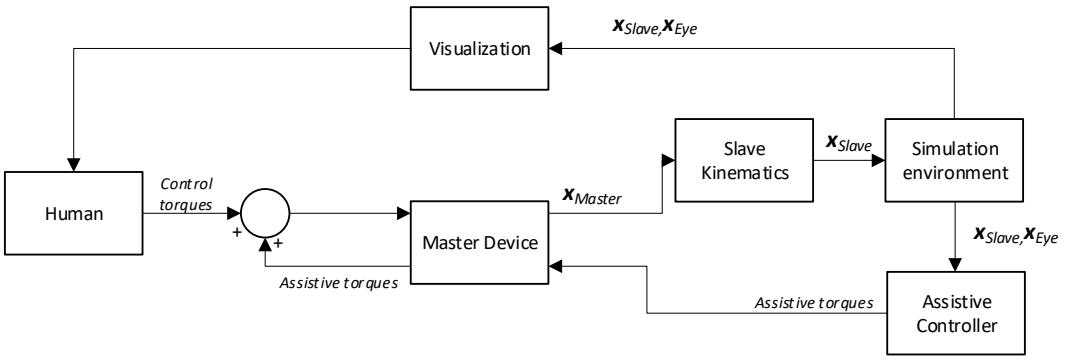

Figure 3.1: Flow chart of the model architecture

3.1.2. Master Device

The instrument manipulator of the PRECEYES Surgical System has 4 Degrees-of-Freedom (DOF) which are used to manipulate the instrument. To realistically simulate this manipulator, the Haptic Master For Needle Steering is used (see Figure 3.2. This device has 3 DOF (one linear translation and two rotations perpendicular to the linear direction), which is sufficient to simulate the procedure. The Haptic Master is actuated in all degrees of freedom which facilitates the application of Shared Control. Originally the device was designed to control a steerable needle that is being developed at Delft University of Technology [14].

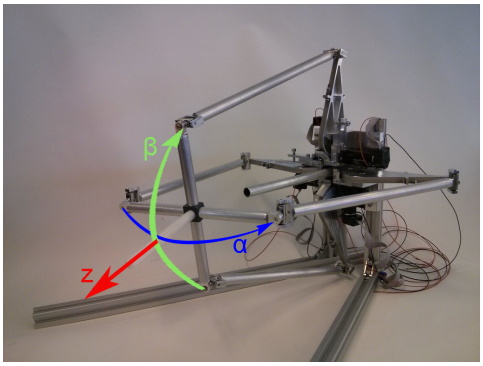

Figure 3.2: The Haptic Master for Needle Steering and the DOF's illustrated

Despite the missing DOF, the Haptic Master is still suitable for this experiment. This is because the task that is simulated does not require this rotational DOF (see 3.2). For more detailed information regarding the Master Device the reader is referred to Appendix A.

3.1.3. Bachmann Controller

The Haptic Master Device is controlled using a real-time Bachmann® controller [1]. The Bachmann controller can send, process and receive digital signals as well as analog signals. The controller reads the digital signal of the four encoders, and generates analog signals that control the master device's actuators. The control architecture inside the Bachmann controller can be programmed using the Simulink® environment in MATLAB®. The M-Target® software developed by Bachmann compiles the Simulink model and installs it on the Bachmann controller. For a schematic layout of the connection between the Bachmann controller and the Master device the reader is referred to Appendix A.

3.1.4. Simulated Environment

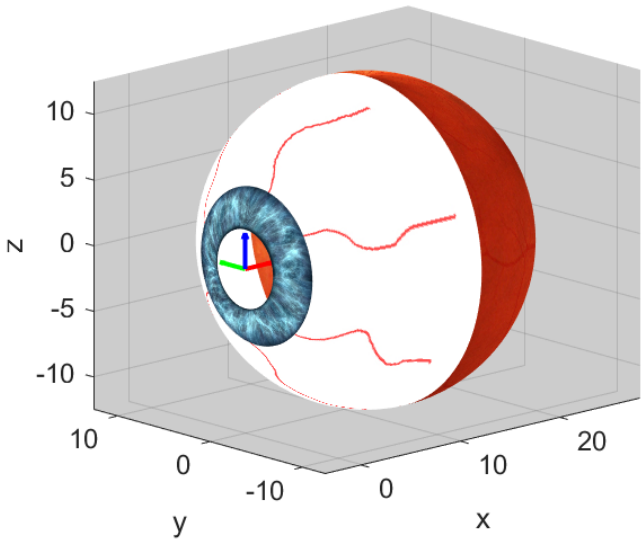

Figure 3.3: 3-d plot of the simulated eye. The colored arrows indicate the origin of the simulation reference frame and the direction of the axes

In order to simulate vitreoretinal surgery a virtual model of the eye is required. Since the focus of this study is application of haptic feedback, a fairly simple model is sufficient. The eye is modeled as a sphere (see Figure 3.3), with a graphic representation of the retina, the outside of the eye and the iris. The pupil is simply

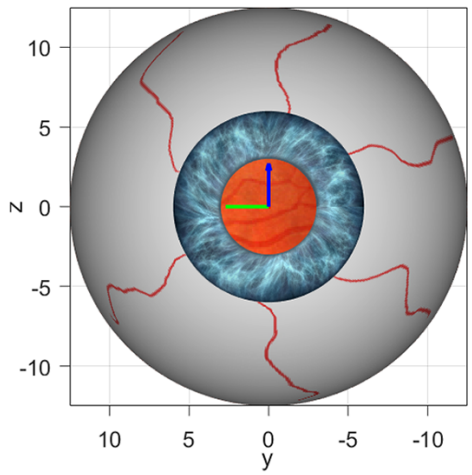

Figure 3.4: Front view of the eye

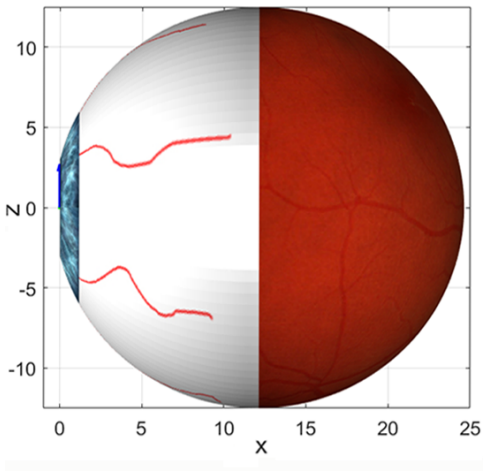

Figure 3.5: Side view of the eye

modeled as a hole in the sphere. The axes in Figure 3.3 are to scale, 1 step in the simulation reference frame represents 1 mm. The green, red and blue arrows start at the origin and show the direction of the x-, y- and z-axis respectively. The radius of the sphere is 12.5 mm, which is based on the average eye ball size [29]. The important parameters of the eye are summarized in Table 3.1

When looking at the virtual representation of the eye in Figure 3.3 it can be seen that the back of the eye

Table 3.1: Eye properties

Property [unit]	Value
Eye center coordinates [mm]	[12.134;0;0]
Eye radius [mm]	12.5
Iris radius [mm]	6
Pupil radius [mm]	3

has a red colour. In fact, it's an image of the retina. One would expect this part of the eye to be white (at least seen from this perspective). However, since the surgeon will be looking straight into the eye (just like in vitreoretinal surgery) he will never see this part of the eye. The vantage point of the surgeon is shown in Figure 3.4. In Figure 3.5 it can be seen that the origin is chosen in such a way that that the yz-plane coincides with the hole that represents the pupil.

3.1.5. Slave Properties

In this experimental set-up the physical master is controlling a simulated slave in a virtual environment. The slave is mimicking a simple surgical pick. The surgical pick is plotted in its local reference frame in Figure 3.6 and 3.7. The properties of the surgical pick are summed up in Table 3.2. The position plotted corresponds to the master being in the neutral position ($\alpha = 0$, $\beta = 0$ and $z = 0$). The mapping of the master pose to the slave pose is given by Equation 3.1, 3.2 and 3.3.

$$\alpha_{slave} = \alpha_{master} \cdot s_f \tag{3.1}$$

$$\beta_{slave} = \beta_{master} \cdot s_f \tag{3.2}$$

$$x_{slave} = z_{master} \cdot 0.04 + x_{base} \tag{3.3}$$

where z_{master} is measured in millimeters. Notice that the z-axis of the master device is translated to an elongation along the x-axis of the slave device. This is counter-intuitive, but for other calculations this reference frame was more convenient. The two rotational DOF's are simply mapped with a scale factor. The translational DOF however is simulated by keeping the Center of Rotation fixed in the origin whilst elongating or shortening the shaft of the instrument. This represents the insertion or the retraction of the instrument from the eye. The Center of Rotation is placed where the instrument enters the eye through the trocar, just like the

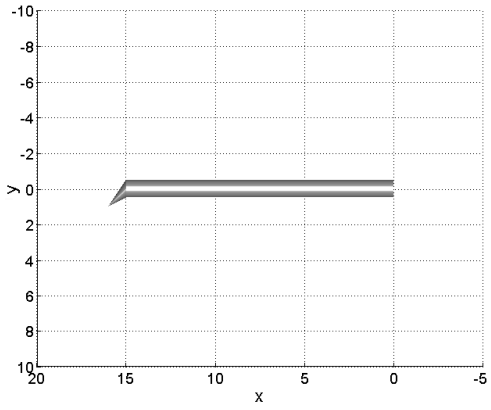

Figure 3.6: The instrument in 2-D plotted in the instrument reference frame

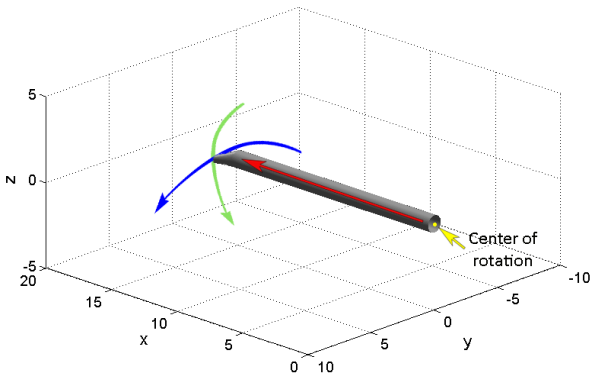

Figure 3.7: 3-D plot of the instrument including the DOF's (colors correspond to Figure 3.2

instrument during real robotic surgery.
Using Equation 3.1-3.2 combined with the range of motion of the master device, the range of motion of the slave device can be calculated. The range of motion and other important slave properties are listed in Table 3.2

Table 3.2: Slave properties

Property [unit]	**Value**
Shaft diameter [mm]	1
Center of rotation [-]	[0;0;0]
Shaft base length x_{base} [mm]	15
tip coordinates (neutral position) [-]	[16;1;0]
tip radius [mm]	0.2
Scaling Factor s_f [-]	0.6
α_{slave} range of motion [°]	-12 to 12
β_{slave} range of motion [°]	-12 to 12
x_{slave} range of motion [cm]	15 to 27

3.1.6. Mapping of slave in simulation reference frame

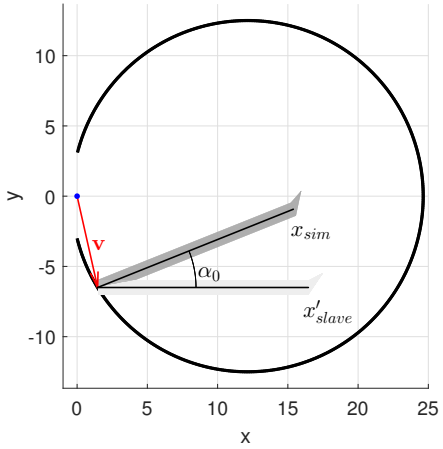

Figure 3.8: Mapping of the instrument in the simulation reference frame. First a rotation occurs, after which a translation places the instrument at the right entry point

The mapping of the slave into the simulation reference frame occurs by means of a rotation and a translation. In the neutral position, the instrument has an angle α_0 with the x-axis shown in Figure 3.8. The translation moves the center of rotation to the entry point of the instrument. Therefore the position of the slave in the simulation reference frame can be calculated using Equation 3.4, 3.5, 3.6 and 3.7. The values of $\mathbf{v}$ and α_0 are given in Table 3.3.

$$\alpha_{sim} = \alpha_{master} \cdot s_f + \alpha_0 \tag{3.4}$$

$$\beta_{sim} = \beta_{master} \cdot s_f \tag{3.5}$$

$$x_{slave} = z_{master} \cdot 0.04 + x_{base} \tag{3.6}$$

$$Center of Rotation = \mathbf{v} \tag{3.7}$$

Table 3.3: Simulation parameters

Property [unit]	Value
α_0 [°]	21.8
$\mathbf{v}$	[1.46;-6.5;0]

3.1.7. Spherical coordinates

In our model the eye is modeled as a sphere. Therefore it is very convenient to express the instrument tip position in spherical coordinates. This will give us a very intuitive idea of the position of the instrument relative to the eye. The orientation of the spherical coordinate system relative to the simulation coordinate system is shown in Figure 3.9. What is not depicted in the figure is that the origin of the spherical reference frame coincides with the center of the eye. This means that the origin is translated along the x-axis when moving from Cartesian to spherical coordinates.
The r-component of the spherical coordinates gives us the distance between the instrument tip and the center of the eye. However, it would be convenient to know the perpendicular distance of the instrument tip to the retina. This value is obtained using Equation 3.8

$$r_{retina} = R_{eye} - r_{spherical} \tag{3.8}$$

where R_{eye} is the radius of the eye. From now on r refers to r_{retina}.

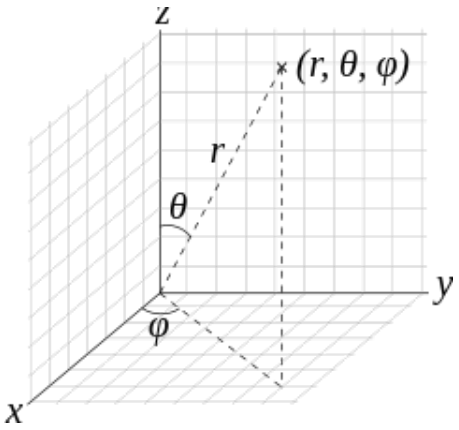

Figure 3.9: The spherical coordinates are shown how they compare to the Cartesian coordinates. The origin is translated to the center of the eye for the spherical coordinates

3.1.8. Total simulation

Now that the master, slave and simulation properties have been defined it is possible to integrate the system. The visualization with the instrument integrated is given in 3.10. An important detail to note is the shadow of the instrument. During vitreoretinal surgery, surgeons rely heavily on this shadow to estimate the distance to the back of the eye. Therefore, to realistically simulate this type of surgery, the shadow must be visualized as well. The yellow target ring can be seen as well, which will be further explained in Section 3.2

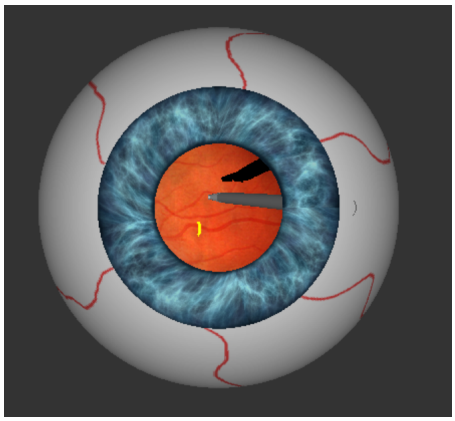

Figure 3.10: An overview of the final simulation from the participant's point of view

3.2. Experimental Design

In order to evaluate the performance of the system an experimental task has to be designed that is comparable to ERM peeling. In order to design a good task, the critical aspects of ERM peeling are determined and analyzed.

Close to retina
In order to peel the membrane, the instrument has to be moved close to the retina.

Preventing damage to retina
While the membrane has to be peeled of the retina, damage to the retina must be prevented

No Force feedback
The forces exerted on the instrument and surgeon are negligible, which means that the surgeon has to rely on his vision.

Peeling motion
The instrument has to move over the membrane with a certain velocity in order to peel it off.

Lack of depth perception

Because of before-mentioned reasons the surgeon has a hampered depth perception, making the procedure more difficult to perform

An experimental task is designed that takes these criteria into account. It consists of a yellow target ring that is placed on the surface of the retina. The target is a yellow semi-circle with a large (0.7 mm) or small (0.3 mm) radius. The participant has to move the instrument tip through the target circle without puncturing the retina. The target circle orientated on the x-z plane, which means the participant has to move the instrument through the circle with a rotation around the z-axis (the α Degree of Freedom). Furthermore, the participant has to move the instrument to the target with a certain positive rotational velocity, meaning the instrument has to move through the ring from right to left in Figure 3.10.
Because of this required velocity, the participants are required to make a 'peeling' motion. It will also force them to be accurate while moving the instrument. Since the target is close to the retina and the participant is not experiencing force feedback, the other requirements are met as well. The target properties are summed up in Table 3.4.

Table 3.4: Target properties

Property [unit]	Value
Small target radius [mm]	0.3
Large target radius [mm]	0.7
Target center θ [rad]	1.74
Target center ϕ [rad]	0.17
Target center r [mm]	12.5
rotational velocity $\dot{\alpha}$ [rad/s]	0.1

3.2.1. Experimental Protocol

The experiment is conducted with 16 participants (15 male, 1 female, aging 24-27). Each participant is informed about the risks of participation and has signed a written consent form (see Appendix **??**. The experiment consists of four different conditions: Small target/no damping, small target/damping, big target/no damping and big target/damping. The participants are asked to perform 10 successful runs per conditions. If a retina puncture occurs, the run is restarted and does not count for the total number of runs. The participants get 3 trial runs per conditions to prevent a learning effect from influencing the experiment. Furthermore, the order of configuration is balanced using a Latin Square. To prevent the participants from getting confused about the damping, they will perform the runs with/without damping consecutively. This means that 8 participants executed the two conditions with damping first, and vice versa. After completing the experiment, the participants filled in a questionnaire (see Appendix **??**.

3.3. Design options for Haptic Assistance

A number of concepts have been elaborated for the assistance design. In this section the different designs are introduced and evaluated.

3.3.1. Virtual wall

One of the designs that was proposed was imposing a virtual wall which would make it (almost) impossible for the instrument to travel into the forbidden region. The forbidden region would be set on the boundary of the retina, therefore preventing retina punctures. As explained in 2.4, the virtual wall would be modeled as a spring with a high stiffness. The area 'outside' the eye is marked as a forbidden region, as can be seen in Figure 3.11 A clear advantage of the virtual wall is that the surgeon can move around freely on the surface

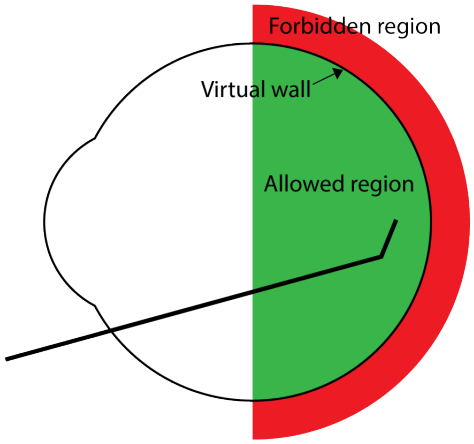

Figure 3.11: The virtual wall as it would be implemented for vitreoretinal surgery

on the retina, as he would be stopped when moving through the retina. Indeed, if the environment would be completely known this would be a very convenient solution. Unfortunately this is not the case. Every human is uniquely defined in its biological structures and therefore every eye is different. It would be impossible to place the virtual wall at exactly the right position. The only position information that is available is the measured distance along the instrument axis by the OCT sensor (see Section 2.2.2). The variation in this sensor is too high to position the virtual wall (the epiretinal membrane is 60 μm thick, and the variation in the sensor is 40 μm). Furthermore, it is not known if the measured distance is perpendicular to the retina or at an angle, since the measurement is performed along the axis of the instrument. Although the virtual wall could be very beneficial in the future, when sensors have improved and the environment is better defined, with the current limitations it is not possible.

3.3.2. Dynamic Damping Field

While considering the virtual wall it occurred that the position of the instrument is *approximately* known. Therefore a concept is designed that does not require an exact position of the instrument. For a dynamic damping field this is the case. The motion of the slave is increasingly dampened as the instrument tip gets closer to the retina. The damping field has two benefits: first of all it slows down motion as the instrument gets closer to the retina, therefore increasing safety. Secondly, the damping field will give the surgeon an intuitive sense of distance that the instrument tip has to the retina. A visual representation of the damping field is given in Figure 3.12.

3.3.3. Final Design:Z-axis Dynamic Damping Field

The Dynamic Damping Field enables users to estimate the instrument position relative to the retina, while it naturally slows down the motion. One property that occurred during the evaluation of the Dynamic Damping Field is that while the damping in the translational direction is very convenient to prevent punctures, the rotation damping is experienced as limiting. Therefore another design is proposed in which the damping field is only imposed in the translational direction. The rotational DOF's are not dampened. The user can now estimate the position of the instrument, decrease the velocity in the direction of the retina while still being able to perform the peeling motion.

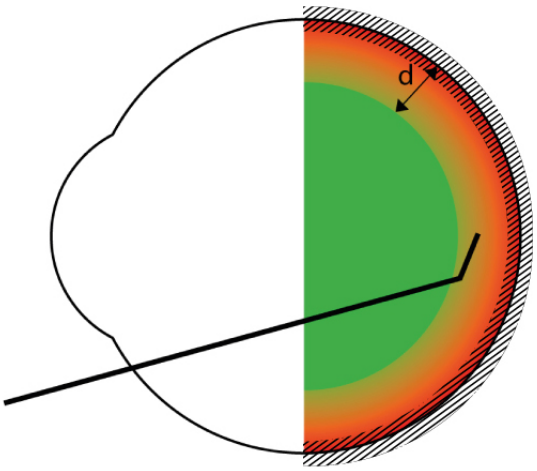

Figure 3.12: The damping field as it would be implemented during vitreoretinal surgery. As the instrument moves closer to the retina the damping field increases. The shaded part indicates the variation in the OCT-sensor

3.3.4. Damping Field properties

The properties of the damping field have been chosen by means of hueristic tuning. The maximum damping coefficient is chosen in such a way that it does not become too dominant, but still is noticeable. The maximum damping coefficient is 10 Ns/mm and linearly decreases as a function of the distance to the retina. The damping field starts at 3 mm from the retina, which is the maximum sensing distance of the OCT sensor. The damping coefficient versus retina distance is plotted in Figure 3.13 The maximum variation in the OCT-

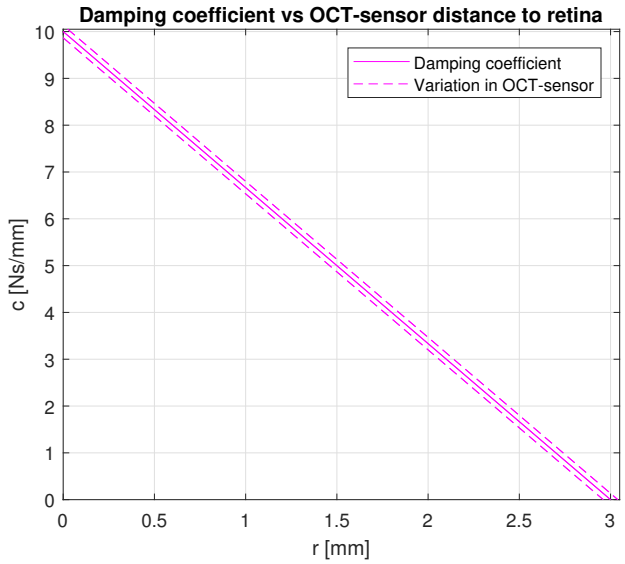

Figure 3.13: The damping coefficient plotted against the measured OCT-sensor distance

sensor (40 μm, see [24]) is plotted in the figure as well. The damping field is linearly increasing because the motion should towards the retina should be dampened and slowed down as the instrument approaches the retina.

4

Results

In this chapter the data collected during the experiment is presented. In Section 4.1 a plot of two typical runs are given. In 4.2 an overview of the number of punctures is given. Section 4.3 summarizes the recorded time per run. The general behaviour and the effect of the damping field per participant is studied in Section 4.4 and finally the safety margin is analyzed in 4.5. A table summarizing the repeated measures ANOVA is given in 4.6.

4.1. Individual runs

In Figure 4.1 a plot is given of two separate runs. The runs are taken from the 'Small Manual' and 'Small Damping' conditions. The four separate plots indicate the four requirements that have to be met in order for a successful target hit. In the top graph the perpendicular distance to the retina is plotted. This distance has to be lower than the radius of the target (plotted as the green dashed line). In the second image, the range for which θ is within the bound is dependent on the value of r. First of all r has to be within the radius of the target. As r gets smaller, the θ-bound gets larger. This is visualized in Figure 4.2. The blue and red dashed

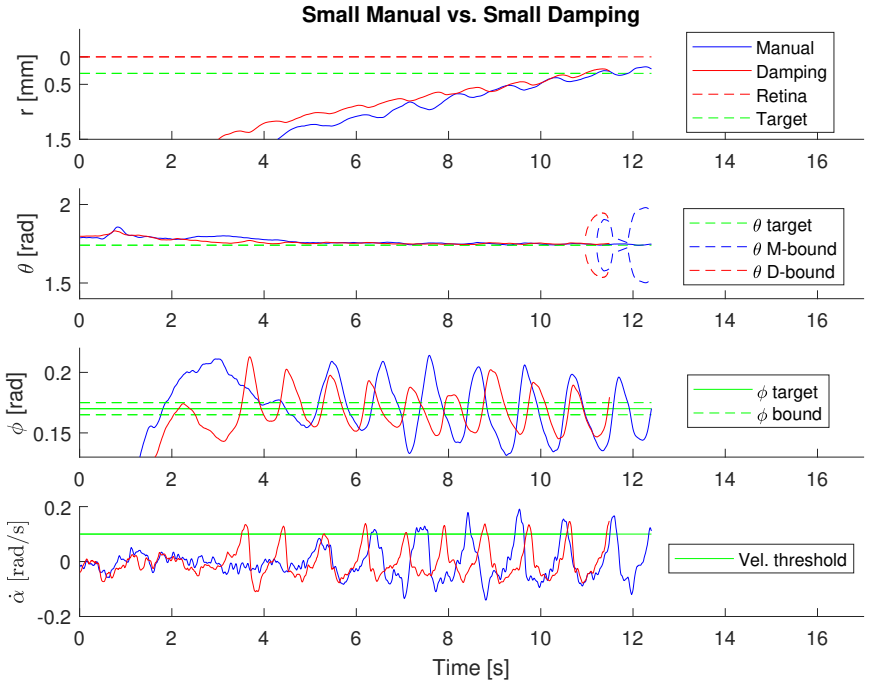

Figure 4.1: Plot of the four separate parameters that need to be satisfied in order to have a successful run

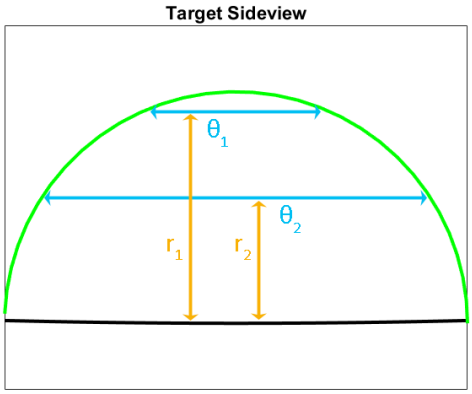

Figure 4.2: Explanation why the θ bound varies as a function of r

lines in Figure 4.1 indicate the theta-bound for the Manual and Dampened runs respectively. The ϕ-bound is simply the 'thickness' of the ring, a bound of 0.01 rad was chosen. The last plot indicates the rotational velocity of the instrument in the α-plane. In order to mimick the peeling motion from right to left, this value has to be above 0.1 rad/s. When looking at the first plot of Figure 4.1, it can be observed that the gradient of the dampened run is lower than the gradient of the manual run. This indicates that the retina is approached in smaller steps. When looking at the ϕ-plot, it can be seen that a peeling motion is made. The instrument is moving from right to left in the horizontal plane to move through the target. In the velocity plot it can be seen that this participant had a correct sense of the required velocity, since almost every attempt is above the velocity threshold at its peak.

4.2. Retina punctures

For each of the four configurations the number of punctures per participant is counted. A 16x4 matrix containing the number of punctures per participant for each condition is obtained. Figure 4.3 shows the distribution of punctures per condition.

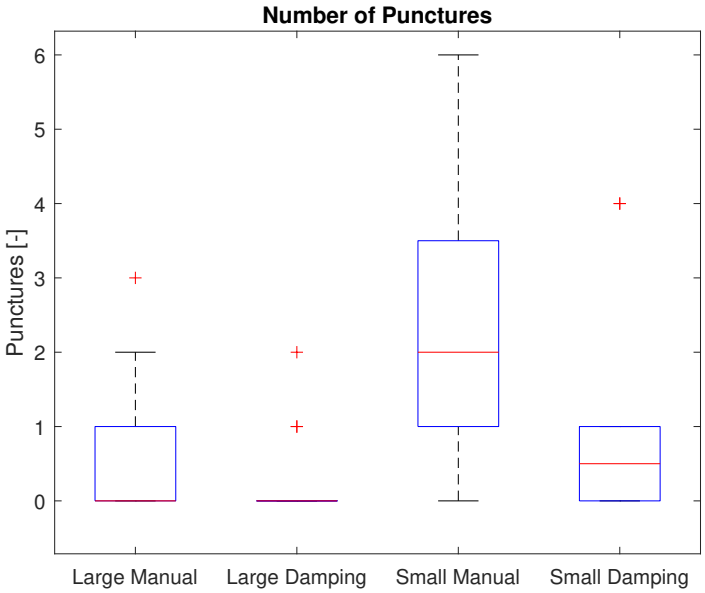

Figure 4.3: Boxplot of the number of punctures for the different conditions

Because some of the metrics are normally distributed (such as time), and some not (number of punctures), a statistical analysis was chosen that can be applied to all metrics. Using [7], the data per metric is ranked from 1 to 64 (16x4). If two values correspond, they both get the same rank number. The obtained rank-transformed matrix is submitted to a repeated measures ANOVA. The four conditions are taken as the within-participant factor. A Bonferroni-corrected post-hoc pairwise comparison is made between the pairs. The results of the repeated measures ANOVA analysis are shown in Table 4.1. A significant difference between the two conditions 'Small Manual' and 'Small Damping' is observed. This indicates that for tasks that require more precision (the small target), the damping field decreases the number of retina punctures and therefore increases safety. On the other hand, no significant difference is observed between 'Large Manual' and 'Large Damping', indicating that when less precision is required, the damping field does not decrease or increase the number of punctures.

4.3. Completion Time

The time that each participant needed to complete a run was recorded. The mean time over 10 runs per condition per participant was taken, which resulted in a 16x4 matrix.
A distinction is made between two different phases during a run: the Approach Phase and the Precise Phase. The transition between the two phases occurs when the perpendicular distance of the instrument to the retina is lower than 1.5 mm. This distance is chosen because it was observed that most participants lower their velocity at this point to be more precise. What can be observed by visual inspection (and confirmed by

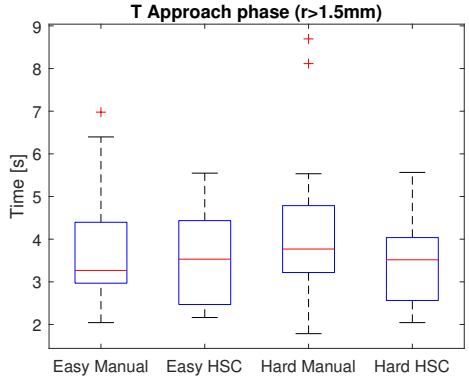

Figure 4.4: Boxplot of the Approach time for the four different conditions

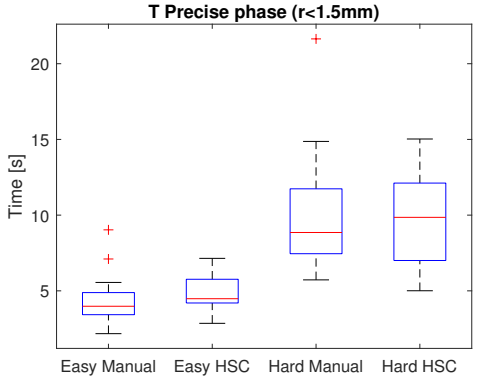

Figure 4.5: Boxplot of the Precise time for the four different conditions

statistical analysis) is that no significant differences arise in the Approach Phase for the different conditions. This is an expected result, since the damping field is only active in the final phase, and the target size mostly influences the final phase due to the required precision. Indeed, if the Precise time is observed, a significant difference between the 'Large' and 'Small' condition is observed. This confirms that the smaller target is indeed harder to perform.

4.4. Effect of damping field on participant behaviour

The number of punctures and the total time are indicators of the effect of the damping field. However, it is also interesting to study the effect of the damping field on the behaviour of the participant during the run. In order to visualize this behaviour, the plot in Figure 4.6 is generated. All the runs for both conditions 'Small Manual' and 'Small Damping' of one participant are plotted in one figure. On the horizontal axis, the perpendicular distance between the instrument tip and the retina is given, divided by the radius of the eye. The left side of the figure is closer to the retina and the target. Because there is a unit of distance on the horizontal axis, the data is normalized and therefore runs of different lengths can be compared. For clarification, the runs start on the right and as time progresses the instrument gets closer to the retina and thus to the left in the plot. The target radius is plotted as well. On the left vertical axis, the derivative of r is plotted, the perpendicular velocity towards the retina. The damping coefficient as a function of r/R is plotted on the secondary axis. When comparing the velocities on the right side of the figure, it can be seen that the velocity for the dampened condition for most runs is higher than the manual condition. This indicates that the participants moves faster through the approach phase, as he is relying on the damping field to indicate that he is getting close to the retina. When looking at the behaviour of the participant as he moves into the damping field, a rapid decrease of velocity is observed. In Figure 4.6 this decrease is marked with a black ellipse. This indicates that the participant is using the damping field to adapt his behaviour to be more precise. Of course, the damping field also decreases $\dot{r}$, since the damping force is working in the translational direction of the instrument. For clarity the data of only one participant is plotted. This behaviour is characteristic for the other participants as well.

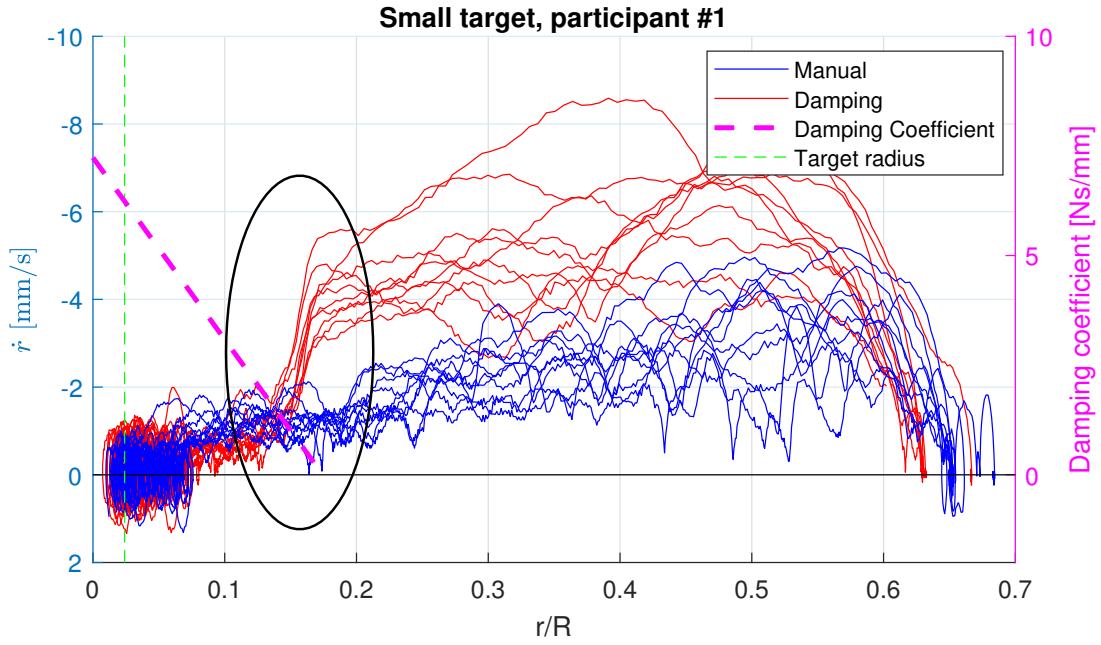

Figure 4.6: All successful runs of one participant plotted in one figure. On the left vertical axis the perpendicular velocity with respect to the retina is plotted. On the secondary axis the damping coefficient is plotted. On the horizontal axis the perpendicular distance to the retina divided by the eye radius

4.5. Sideview of target

In Figure 4.7 and 4.8 the average position of the instrument tip when the target is hit is plotted for all participants. The two conditions with the large target are plotted on the left side, the conditions with the small target are plotted on the right. Note the difference in scale on the axes, which indicates the difference in size for the different targets. The vertical distance to the retina is a metric of interest. The participants were instructed to

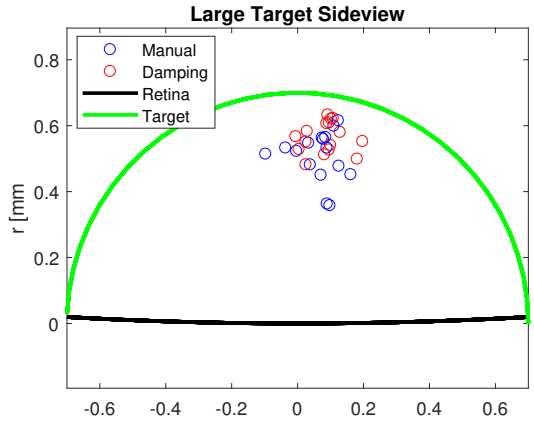

Figure 4.7: Sideview of the large target

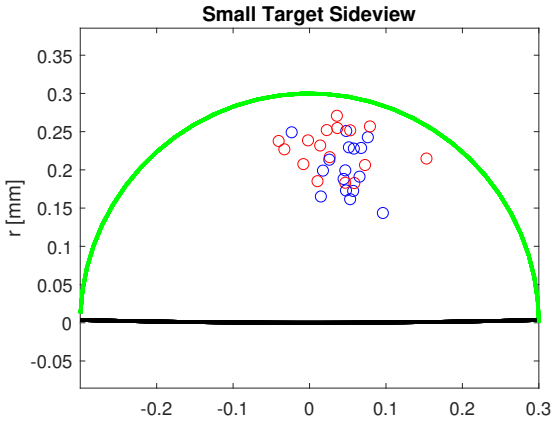

Figure 4.8: Sideview of the small target

prevent punctures, so it is beneficial to keep the distance between the instrument and the retina as large as possible. This distance can be considered as a *safety margin*. For both the large and small target, the manual configuration seems to have a smaller safety margin compared to the dampened configuration. A boxplot for all 4 configurations is given in Figure 4.9. A clear distinction can be seen between the 'Large Target' configurations and the 'Small Target'. This is logical, since a larger safety margin is possible when the target is larger. A repeated measures ANOVA has been performed on the safety margin data and has been reported in Table 4.1. The analysis indicates a significant difference between the 'Small Manual' and 'Small Damping' condition. This means that for the smaller target, participants are able to maintain a larger safety margin when the damping field is activated. For the large target, no significant difference is found. It is understandable that for the smaller target the safety margin is increased, since the distance between the target and the retina is smaller. For the same reason the spread for the large target is wider than the spread for the small target. The radius of the large and small target are plotted as well to indicate the maximum safety margin.

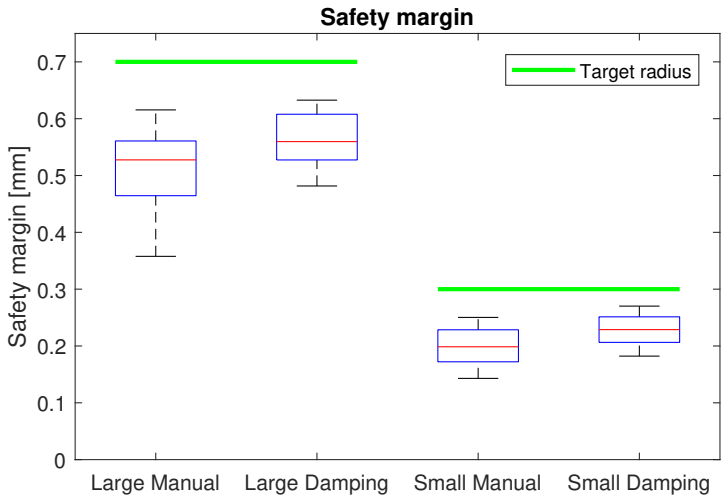

Figure 4.9: Boxplot of the safety margin for the different conditions

4.6. ANOVA Results

The results of the repeated measures ANOVA and pair-wise comparison are reported in Table 4.1.

Table 4.1: Summarized results of the repeated measures ANOVA and pair-wise comparison. p<0.05 is considered significant

	Large Manual	Large Damping	Small Manual	small Damping		Pair-wise comparison					
	1	2	3	4							
	M (SD)	M (SD)	M (SD)	M (SD)	p-value F	1-2	1-3	1-4	2-4	2-4	3-4
Punctures (-)	0.63 (0.96)	0.25 (0.58)	2.38 (1.7)	0.88 (1.31)	4.1e−5 F=9.8	1	0.002	1	1.3e−4	0.65	0.03
$T_{approach}$ (s)	3.81 (1.45)	3.51 (1.11)	4.30 (1.85)	3.43 (1.01)	0.166 F=1.7698	1.00	0.27	1.00	0.70	1.00	0.46
$T_{precise}$ (s)	4.40 (1.74)	4.89 (1.30)	9.92 (4.06)	9.82 (3.10)	1.6e−18 F=84.577	1.00	5.4e−7	8.4e−8	5.3e−8	1.8e−8	1.00
Margin (mm)	0.51 (0.07)	0.56 (0.05)	0.20 (0.03)	0.23 (0.03)	1.1e−22 F=137.61	0.13	8e−10	1.1e−7	4e−11	2.6e−9	0.03

5 Discussion

This study investigated the effects of an assistive damping field during robotic vitreoretinal surgery. Now that the data has been analysed in the previous chapter it is time to draw conclusions based on this study. First of all the results given in 4 are analyzed in Section 5.1, followed by a general discussion in Section 5.2. Finally a prospect to future work is given in Section 5.3.

5.1. Results

5.1.1. Retina Punctures

One of the main instructions of the participants was to prevent punctures at all time. Therefore the number of punctures can be considered as a very important metric, since it was a priority of the participants. The decrease of punctures for the 'Small Damping' condition compared to the 'Small Manual' conditions indicates that participants use the damping field in order to increase precision (or at least, prevent punctures). The fact that the number of punctures did not increase for the two conditions with the larger target emphasizes that the damping field is only beneficial when precision is required. It is not surprising that there were less punctures for the bigger target, since the risk of a puncture was much smaller. One could argue that if this result would be extrapolated to a smaller target, an even larger decrease in punctures could be observed. However, this can not be assumed and would be an interesting topic for further studies.

5.1.2. Time to Completion

Although time was not an explicit priority for the participants it is still a good indicator of the performance of the participants. For both the approach phase and the precise phase no significant differences were found between the dampened and manual conditions. A small decrease is observed in he approach phase for the two dampened conditions, but this is too small to be significant. This was not an expected result, but at least it indicates that the damping field does not limit the performance. Combined with the number of retina punctures the damping field produces less punctures in the same completion time for the small target. The time analysis does confirm that the small target was harder to complete successfully than the large target.
One of the limitations of the time analysis is that the participants were not instructed to perform the experiment as fast as possible. This was a conscious trade-off, since the participants can not focus at two goals at the same time (prevent punctures and be as fast as possible), especially since those two are contradictory. However, it would be nice to think of an experimental set-up in which the participants would focus on both these goals. For example a scoring system could be introduced where you score points based on your completion time, but in case of a puncture points would be deducted. Although this would prioritize time ánd punctures, the task would stray away from the original purpose: to mimick ERM peeling.

5.1.3. Participant behaviour

Some general conclusions can be drawn when looking at the overall behaviour of the participants. When looking at Figure 4.1, in which two individual runs (dampened and manual) are plotted, it can be observed that the dampened run approaches the retina in smaller steps. Because these steps are smaller, the chance of a retina puncture becomes smaller. This decrease in step size can be seen as a direct consequence of the damping field, since this dampens the motion in the direction of the retina.

In Figure 4.6 the behaviour of one participant is summarized for all runs. This figure indicates the difference between the manual runs and the dampened runs. When looking at the dampened runs, it can be observed that the participant is actually relying on the damping field. He is moving faster through the initial phase, and as soon as he encounters the damping field the velocity is decreased. The decrease in velocity occurs at approximately the same point for all runs, which indicates that the perception of the participant of the damping field is quite accurate.
Because this participant moves faster through the approach phase, one would expect that the approach time is lower for the dampened phase. However this is not the case. This can be explained due to the variety of behaviour between participants. As said, the examined behaviour is typical for most participants, but some participants showed different behaviour. While most participants considered the damping field as convenient, some participants experienced it as limiting and this is also reflected in their performance. Of course, this is not surprising. When working with humans one should expect high variance between participants. It was observed in the experiment that the damping field increased the performance of most participants, but some performed worse.

5.1.4. Safety margin

In the previous section it was concluded that the participants reduced their velocity when they encountered the damping field. Although this is an indication that the participants relied on the damping field, it does not indicate whether the participants use the damping field to estimate the distance to the retina (which is, after all, is the purpose of the damping field). It could be the case that the participants only use the beginning of the damping field to decrease their velocity, after which they rely on their visual senses again.
The safety margin is a better indicator whether the participants have an understanding of the distance to the retina. The increase in the safety margin for both dampened cases indicate that the participants use the damping field to estimate distance, or at the very least exploit the damping field to approach the retina as slow as possible. When looking back at the actual procedure (ERM peeling), this is of course beneficial behaviour. During ERM peeling one wants to make contact with the retina with as little velocity as possible.

5.2. General discussion

5.2.1. Damping field

This study was executed as a exploratory study. The main question was *whether* a damping field would improve precision. Now that it is indicated that robotic vitreoretinal surgery could benefit from a dynamic damping field, it is time to consider in what way the damping field should be applied. For this study a very simple, linear increasing damping field was applied. No variations were studied in the design of the damping field. Some suggestions for the damping field are summarized below:

Exponential increase The current damping field had a linearly increase as the instrument approached the retina. It would be interesting to see whether the results would improve when an exponentially increasing damping field would be imposed. The damping would be higher in the final phase, which could possibly lead to higher precision.

Maximum damping The maximum damping coefficient for this study was determined through hueristic tuning. No experiments were performed in order to quantify the performance of different damping coefficients. An experiment with different maximum dampings could be performed in order to compare different damping coefficients.

Step increase The current damping field comes up gradually as the instrument moves closer. Another option to consider is to put a step increase at the start of the damping field. The user would then feel a sudden increase in damping as he moves into the damping field. Since it was observed that participants respond to the beginning of the damping field, this could be an interesting effect

Decrease damping field size Right now the damping field starts at a (measured) distance of 3 mm. This turned out to be quite far as the critical zone is closer to the retina. Moving the damping field closer to the retina will focus the damping field, and provide assistance in the right place.

In a future study the above-mentioned factors can be combined to design a better damping field.

5.2.2. Experimental set-up

While setting up the experiment, all precautions have been taken to prevent unwanted effects to influence the results. The experiment is designed in such a way that several metrics could be singled out. Any variation in these metrics should be caused by the studied factor, and the experiment itself should not introduce any bias. However, during the experiment some undesired effects were observed. In general, participants made more mistakes (punctures) in the first 20 runs than in the last 20 runs. This indicates that the training period was too short, and that the participants were still learning during the experiment. Although this is an undesired effect, it did not influence the experiment that much. This is due to the Latin Square sorting of the experiment. The Latin Square order ensured that every possible order of configurations was executed twice. Therefore the learning effect influenced each factor equally. Still, for more accurate results it would be beneficial to extend the training period.
Another choice that was made was to fix the target location. This choice was made because this made it very easy to compare different runs to each other. It was not considered that the OCT-sensor behaves differently in different parts of the eye. This is due to the fact that the OCT sensor measures along the axis of the instrument, because the sensor is measuring at an angle. This measurement can differ a lot from the actual perpendicular distance between the retina and the instrument. It would have been interesting to see the behaviour of the damping field in different parts of the eye, when the measurement difference would be different. Another benefit from switching the target location is that in the current set-up, the measurement error is always the same. It does not vary for a certain location, so participants would get used to a damping field in a certain area. By changing the location the participants would have to adapt to the different damping field properties and this would probably have an effect on the performance.

5.2.3. Variation in OCT-sensor

Due to an error in units, the effect of the variation in the OCT-sensor was negligible. This is a pity, since it would have been incredibly valuable to study the effect of the OCT-sensor variation on the damping field and the performance of the participants. In a previous study the performance of the OCT-sensor has been analysed, so its behaviour could be readily implemented in a future study. In this study it has been shown that despite a small deviation in the distance measurement, the participants were still able to work more precise. However, this deviation was constant, not varying like the OCT sensor measurement.

5.2.4. Simulation limitations

When simulating a 'real-world' problem one always has to make design choices and trade-offs between realism and practicality. Certain assumptions are made that on one hand simplify the problem, but on the other hand reduce the applicability. Key is to identify the important factors for the problem at hand, and making sure these factors are represented properly in the simulation. This study was mainly focused on the part of the procedure before contact is made. Therefore almost no tissue properties have been taken into account, because this experiment stopped at the moment of contact. During 'real' ERM peeling, tissue dynamics play an important role. The membrane sticks to the retina, and when contact is made, the retina moves. The retina can detach or get torn. The same goes for the membrane. These mechanism are incredibly complex and it was a concious choice not to take these factors into account. In future studies these factors can be simulated as well, although one can argue if it's worth the effort to simulate this behaviour, or that studying *in vitro* specimens would provide better results and require less effort.
The model of the slave is quite simplified as well. The slave is modeled as a masseless device that perfectly follows the motion of the master. No control delays or inertial dynamics were taken into account. Although it would be more realistic to consider these factors, it is a safe assumption that they would not influence the result that much. The PRECEYES Surgical System is designed to optimize precision and accuracy, and since the instruments at hand are extremely light-weight, the inertial dynamics and delays are very small. Furthermore, the control of the PRECEYES Surgical System is designed to reduce these effects, and the control of the system is considered beyond the scope of this study.

5.2.5. Puncture Velocity

A metric of interest that has not been considered in this report is the velocity of the instrument at the moment a puncture occurs. One could argue that punctures at high velocity cause more damage than punctures at a low velocity. When starting the experiment, it was meant to study the puncture velocity for the different conditions and see if a difference occurs. However, because of the nature of the experiment, different number of punctures and therefore a different amount of data-points per conditions was acquired. This made it very difficult to compare the different conditions. A plot of the different velocities is given in Appendix D. In a future study a format could be considered that would enable more close examination of this metric.

5.2.6. Relation to Current Research

When looking at literature that's available on robotic vireoretinal surgery, most research seems to focus on force sensors. In [3] a control method based on a force sensor is proposed in order to reduce reaction forces during ERM peeling. In [31] an OCT-sensor is integrated in the forceps, and this data is visually displayed to the surgeon. This study combined these promising methods by proposing a control method based on OCT measurements.

5.3. Future work

In this study a first step is put towards assisted robotic vitreoretinal surgery. The question that instigated this research was how the OCT-sensor data could be fed back to the surgeon. In this research it has been shown that haptic assistance by a means of a damping field is a viable option. Of course it is wise to investigate other methods, such as auditory or visual feedback, and compare those results to this study.
As mentioned before, the study has been a qualitative rather than a quantitative, and further research is highly advisable. A number of factors deserve more attention. First of all the damping field design should be reconsidered. In this chapter a number of suggestions to enhance the design have been made, and a lot more sophisticated designs are possible. The simulation can be made more realistically. However, the factors that are of interest for ERM peeling are quite complex to model.
More knowledge can be acquired when the next study would be conducted on the actual surgical system.

Experiments with artificial or porcine eyes is the next logical step. With *in-vitro* specimens a more realistic experiment can be conducted. The system will be exposed to a more dynamic environment and the simplifications that were inherent to this experiment will no longer be of importance.
On the other hand, the simulation built for this study is already there. The parameters of the simulation can be changed easily and more complex designs can be applied. If further study is conducted in this field, the current simulation can be used as a starting point.

6

Conclusion

This study aims to show whether an imposed damping field on a tele-operated robotic surgical system for vitreoretinal surgery can increase safety and accuracy. In order to do so, a simulation is designed which is used to study the effect of the damping field. For the experiment, participants interacted with a physical master that controls a virtual slave in a simulated environment.
The number of retina punctures decreased for the small target. No difference in retina punctures for the large target is observed, and the damping field has no effect on the completion time. There are indications that the participants use the damping field to perceive depth, but this effect should be further studied. It was clearly observed that the participants use the beginning of the damping field as a trigger to decrease their velocity.
A simple linear damping field design is evaluated. A number of parameters that could improve the damping field have been identified, and the effect of these parameters on the performance and depth perception should be further investigated.
In this research a proof-of-concept has been tested that show promising results for implementation on the PRECEYES Surgical System. Another option is to to improve the current simulation, and perform a more realistic experiment. However, more valuable results can be obtained when performing an experiment with the actual surgical system on artificial specimens or porcine eyes.

Bibliography

[1] Bachmann electronic GmbH | Controller System. URL https://www.bachmann.info/en/products/controller-system/.

[2] E. Abdelkader and N. Lois. Internal limiting membrane peeling in vitreo-retinal surgery. *Survey of ophthalmology*, 53(4):368–396, 2008.

[3] M. Balicki, A. Uneri, I. Iordachita, J. Handa, P. Gehlbach, and R. Taylor. Micro-force sensing in robot assisted membrane peeling for vitreoretinal surgery. In *International Conference on Medical Image Computing and Computer-Assisted Intervention*, pages 303–310. Springer, 2010.

[4] M. Balicki, T. Xia, M.Y. Jung, A. Deguet, B. Vagvolgyi, P. Kazanzides, and R. Taylor. Prototyping a hybrid cooperative and tele-robotic surgical system for retinal microsurgery. *MIDAS journal*, 2011:815, 2011.

[5] B.C. Becker, R.A. MacLachlan, L.A. Lobes, and C.N. Riviere. Vision-based retinal membrane peeling with a handheld robot. In *Robotics and Automation (ICRA), 2012 IEEE International Conference on*, pages 1075–1080. IEEE, 2012.

[6] A. Bettini, P. Marayong, S. Lang, A.M. Okamura, and G.D. Hager. Vision-Assisted Control for Manipulation Using Virtual Fixtures. *IEEE Transactions on Robotics*, 20(6):953–966, dec 2004. ISSN 1552-3098. doi: 10.1109/TRO.2004.829483. URL http://ieeexplore.ieee.org/document/1362691/.

[7] W.J. Conover and R. L. Iman. Rank transformations as a bridge between parametric and nonparametric statistics. *The American Statistician*, 35(3):124–129, 1981.

[8] M. Dewan, P. Marayong, A.M. Okamura, and G.D. Hager. Vision-based assistance for ophthalmic microsurgery. In *International Conference on Medical Image Computing and Computer-Assisted Intervention*, pages 49–57. Springer, 2004.

[9] K.M. Fargen, R.D. Turner, and A.M. Spiotta. Factors That Affect Physiologic Tremor and Dexterity During Surgery: A Primer for Neurosurgeons. *World Neurosurgery*, 86:384–389, 2016. ISSN 18788750. doi: 10.1016/j.wneu.2015.10.098.

[10] S. Fraser-Bell, M. Guzowski, E. Rochtchina, J.J. Wang, and P. Mitchell. Five-year cumulative incidence and progression of epiretinal membranes: the Blue Mountains Eye Study. *Ophthalmology*, 110(1):34–40, jan 2003. ISSN 0161-6420. URL http://www.ncbi.nlm.nih.gov/pubmed/12511343.

[11] P.K. Gupta, P.S. Jensen, and E. de Juan Jr. Surgical forces and tactile perception during retinal microsurgery. In *Lecture Notes in Computer Science*, volume 1679, pages 1218–1225. Springer, 1999. ISBN 978-3-540-66503-8. doi: 10.1007/10704282. URL http://www.springerlink.com/index/10.1007/10704282.

[12] X. He, M. Balicki, P. Gehlbach, J. Handa, R. Taylor, and I. Iordachita. A novel dual force sensing instrument with cooperative robotic assistant for vitreoretinal surgery. In *Robotics and Automation (ICRA), 2013 IEEE International Conference on*, pages 213–218. IEEE, 2013.

[13] X. He, M Balicki, P. Gehlbach, J. Handa, R. Taylor, and I. Iordachita. A multi-function force sensing instrument for variable admittance robot control in retinal microsurgery. In *2014 IEEE International Conference on Robotics and Automation (ICRA)*, pages 1411–1418. IEEE, 2014.

[14] A.G.L. Hoevenaars, P. Lambert, and J.L. Herder. Kinematic design of two elementary 3dof parallel manipulators with configurable platforms. In *Computational Kinematics*, pages 315–322. Springer, Dordrecht, 2014.

[15] T. Horeman. Force-based assessment of tissue handling skills. 2014.

[16] L.M. Kranendonk. What haptic technologies could improve robotic vitreoretinal surgery, and which are the most promising?, 2017.

[17] T. Meenink, G. Naus, M. de Smet, M. Beelen, and M. Steinbuch. Robot assistance for micrometer precision in vitreoretinal surgery. *Investigative Ophthalmology & Visual Science*, 54(15):5808–5808, 2013.

[18] S.S. Nudehi, R. Mukherjee, and M. Ghodoussi. A shared-control approach to haptic interface design for minimally invasive telesurgical training. *IEEE Transactions on Control Systems Technology*, 13(4):588–592, jul 2005. ISSN 1063-6536. doi: 10.1109/TCST.2004.843131. URL http://ieeexplore.ieee.org/document/1453568/.

[19] A.M. Okamura. Haptic feedback in robot-assisted minimally invasive surgery. *Current opinion in urology*, 19(1):102–7, jan 2009. ISSN 1473-6586. doi: 10.1097/MOU.0b013e32831a478c. URL http://www.ncbi.nlm.nih.gov/pubmed/19057225http://www.pubmedcentral.nih.gov/articlerender.fcgi?artid=PMC2701448.

[20] J.W. Park, J. Choi, Y. Park, and K. Sun. Haptic Virtual Fixture for Robotic Cardiac Catheter Navigation. *Artificial Organs*, 35(11):1127–1131, nov 2011. ISSN 0160564X. doi: 10.1111/j.1525-1594.2011.01373.x. URL http://doi.wiley.com/10.1111/j.1525-1594.2011.01373.x.

[21] G.A. Peyman, S.A. Meffert, F. Chou, and M.D. Conway. *Vitreoretinal surgical techniques*. CRC Press, 2000.

[22] J. Ren, R.V. Patel, K.A. McIsaac, G. Guiraudon, and T.M. Peters. Dynamic 3-D Virtual Fixtures for Minimally Invasive Beating Heart Procedures. *IEEE Transactions on Medical Imaging*, 27(8):1061–1070, aug 2008. ISSN 0278-0062. doi: 10.1109/TMI.2008.917246. URL http://ieeexplore.ieee.org/document/4579344/.

[23] L.B. Rosenberg. The Use of Virtual Fixtures as Perceptual Overlays to Enhance Operator Performance in Remote Environments. Technical report, Stanford Univ. CA Cent. Des. Res., 1992.

[24] R.J. Samplonius, Y. G. M. Douven, M. J. G. van de Molengraft, and M. Steinbuch. Distance Measurement and Retinal Recognition from A-scans using an OCT Probe. 2017.

[25] N.J.P. Van De Berg. Needle Steering Mechanics and Design Cases. jan 2016. doi: 10.4233/UUID:BDB314B6-9346-4054-9962-D7038999B3AD. URL https://repository.tudelft.nl/islandora/object/uuid:bdb314b6-9346-4054-9962-d7038999b3ad?collection=research.

[26] C Wagner, N Stylopoulos, and R Howe. Force feedback in surgery: Analysis of blunt dissection. In *Proceedings of the 10th symposium on haptic interfaces for virtual environment and teleoperator systems*, 2002.

[27] S. Wang. Integration of a Needle Haptic Telemanipulation System. Master thesis, Delft University of Technology, 2016. URL uuid:99ee4735-91fe-4682-9f56-ee44cd4e101f.

[28] J.R. Wilkins, C.A. Puliafito, M.R. Hee, J.S. Duker, E. Reichel, J.G.. Coker, J.S. Schuman, E.A. Swanson, and J.G. Fujimoto. Characterization of Epiretinal Membranes Using Optical Coherence Tomography. *Ophthalmology*, 103(12):2142–2151, 1996. ISSN 01616420. doi: 10.1016/S0161-6420(96)30377-1.

[29] James G Wong, Nitin Sachdev, Paul E Beaumont, and Andrew A Chang. Visual outcomes following vitrectomy and peeling of epiretinal membrane. *Clinical and Experimental Ophthalmology*, 33(4):373–378, aug 2005. ISSN 1442-6404. doi: 10.1111/j.1442-9071.2005.01025.x. URL http://doi.wiley.com/10.1111/j.1442-9071.2005.01025.x.

[30] T. Yamamoto, N. Abolhassani, S. Jung, A.M. Okamura, and T.N. Judkins. Augmented reality and haptic interfaces for robot-assisted surgery. *The International Journal of Medical Robotics and Computer Assisted Surgery*, 8(1):45–56, mar 2012. ISSN 14785951. doi: 10.1002/rcs.421. URL http://doi.wiley.com/10.1002/rcs.421.

[31] H. Yu, J. Shen, R.J. Shah, N. Simaan, and K.M. Joos. Evaluation of microsurgical tasks with oct-guided and/or robot-assisted ophthalmic forceps. *Biomedical optics express*, 6(2):457–472, 2015.

A

Master device and Bachmann Controller

Originally the device was designed to control a steerable needle that is being developed at Delft University of Technology [14].

The available Degrees-Of-Freedom are shown in A.1. The arrows indicate the positive direction. The two rotational directions (α in the horizontal plane, β in the vertical plane) have a minimum and maximum deflection of -20 ° and +20 °. The device can move up from 0 to 20 cm in the z-direction.

Table A.1: Master device properties

Property [unit]	Value
α_{master} range of motion [°]	-20 to 20
β_{master} range of motion [°]	-20 to 20
z_{master} range of motion [cm]	0 to 30
Max. force (translational DOF) [N]	10
Max. torque (rotational DOF) [Nm]	0.3
Encoder resolution [PPR]	4000

The device consists of four legs that are actuated by DC motors (see Figure (A.1). These actuators move the device in the desired position (or express the desired force, depending on the task). Encoders are mounted on top of the actuators. These encoders accurately read the motor positions which are fed back to the controller. Based on these encoders the position of the master device is known at any point in time.

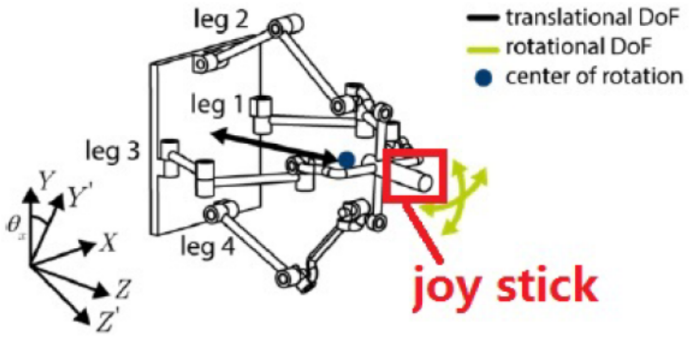

Figure A.1: Schematic drawing of the Haptic Master showing the four legs, the DOF's and the local reference frame [27]

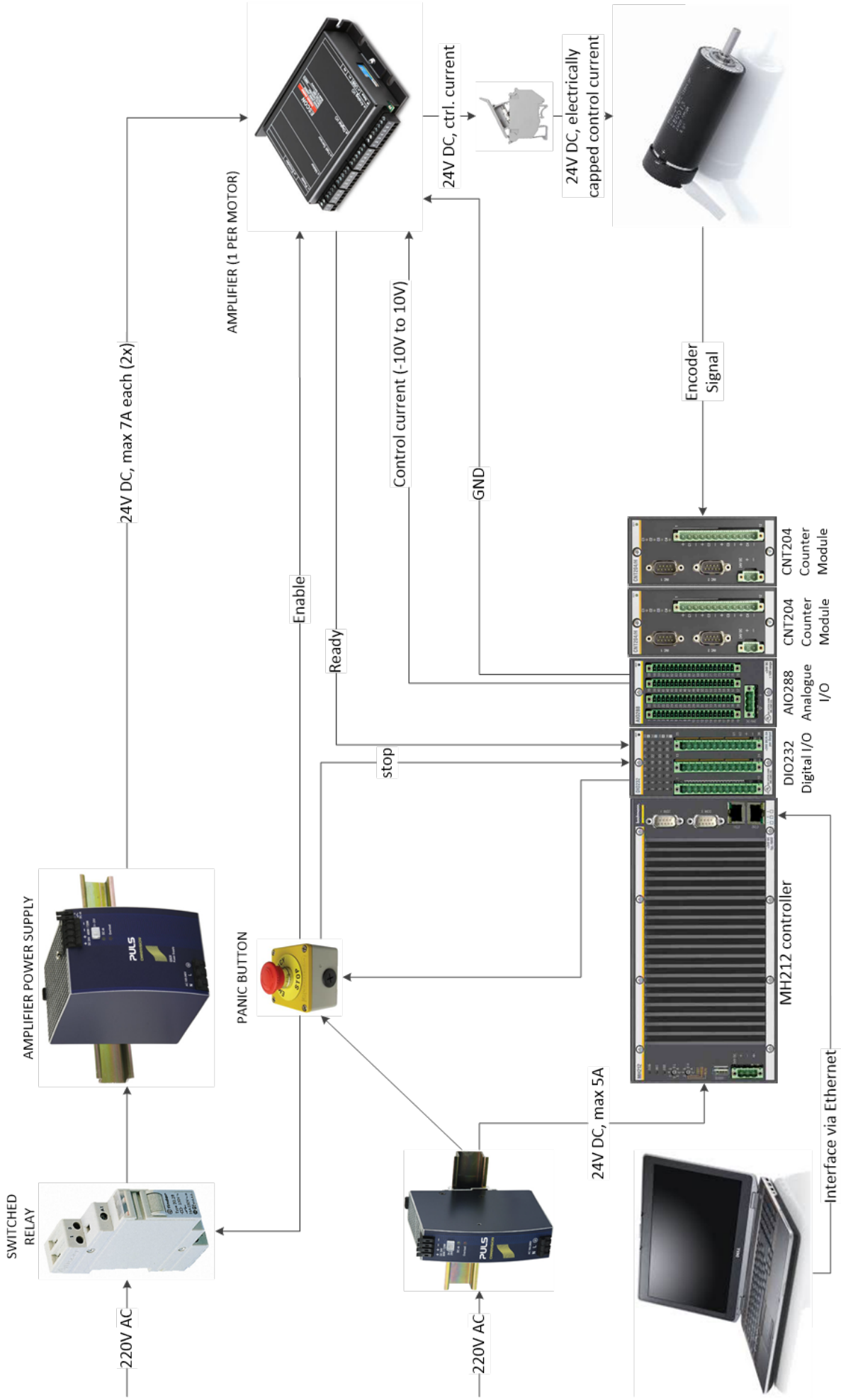

Figure A.2: Schematic lay-out of the master device

B

Informed Consent Form

The form as it has been signed by the subjects is shown on the next two pages.

INFORMED CONSENT FORM

TO PARTICIPATE IN A ROBOTIC SURGERY SIMULATOR EXPERIMENT

Researchers
L.M. Kranendonk, Bsc.
Email: lmkranendonk@gmail.com
Tel: 0621840465

Location of the experiment
Delft University of Technology
Department of Mechanical Engineering
Mekelweg 2, Delft
Haptics Lab, Room 34 F-1-360

Introduction
You are invited to participate in a research study conducted by Laurens Kranendonk on robotic vitreoretinal surgery (surgery on the retina of the eye). Before you agree to participate in this study, it is important that the following explanation of the proposed procedures be read and understood. This document describes the purpose, procedures, benefits, risks, and possible discomforts of the study. It also describes the right to withdraw from the study at any time.

Purpose of the study
The purpose of this experiment is to investigate the effect of haptic assistance on control strategy, performance and user experience during robotic vitreoretinal surgery. You will be using a haptic device to control a simulated robotic instrument. During the experiment, haptic assistance will be provided to help perform the task at hand. You will be performing a task that represents that mimics vitreoretinal surgery.

Duration
The experiment will take approximately 30 minutes to complete

Procedures
Before the start of the experiment you will have the opportunity to get yourself in a comfortable position. You are allowed to move the screen or the haptic device (to a certain extent) in a position that suits you.

At first you will have 6 trials without assistance, and 6 with haptic assistance to get used to the experiment. The aim of the experiment is to move the instrument through a yellow target ring (a more detailed instruction including images will follow).

Once you are used to controlling the system the actual experiment will start. There are 2 difficulty settings (Easy and Hard), and you will perform both with and without haptic assistance, meaning you will perform the experiment in 4 different conditions. Per condition a total number of 10 successful runs are required. A successful run is achieved when the instrument is moved through the target ring at the right speed. When the instrument is moved through the retina it will result in a failure and the trial has to be re-started. A failure will not count as a successful run.

Once you have performed 10 successful runs per condition, the experiment ends and you will receive a short questionnaire.

Risks and discomforts
In some persons, simulators and virtual environments may cause different types of sickness such as visuomotor issues (eyestrain, blurred vision, difficulty focussing), nausea, drowsiness, fatigue, or headache. These symptoms are similar to motion sickness. If you feel uncomfortable in any way, you are advised to stop the experiment. You can stop participating at any time without any negative consequences. If you do not feel well, then please take sufficient rest before leaving the laboratory.

Confidentiality
All the data collected in this study will be kept confidential. Throughout the study you will be identified by a subject number only.

Right to refuse or withdraw
Your participation is strictly voluntary and you may refuse to participate, or discontinue your participation at any time, without negative consequences.

Questions
If you have any questions concerning this study, you may contact Laurens Kranendonk (contact details at the top).

I have read and understood the information provided above.
I give permission to process the data for the purposes described above.
I voluntarily agree to participate in this study.

Name: Date:

Signature of the participant

C

Questionnaire

Given below is the questionnaire as it was filled in by the participants after the experiment

1. Were you able to estimate the distance to the retina using the damping field? (Yes/No+motivation)

2. Which setting was more convenient, Manual or Damping?

3. Did you consider the damping field as limiting or annoying?

4. Could you describe your control strategy for both settings? Indicate if there are any differences

D

Puncture Velocity

In Figure D.1 the puncture velocities per condition are given. Since the number of punctures per condition is different, it is not possible to perform a statistical analysis. It can be observed that for both manual conditions, more high outliers occur.

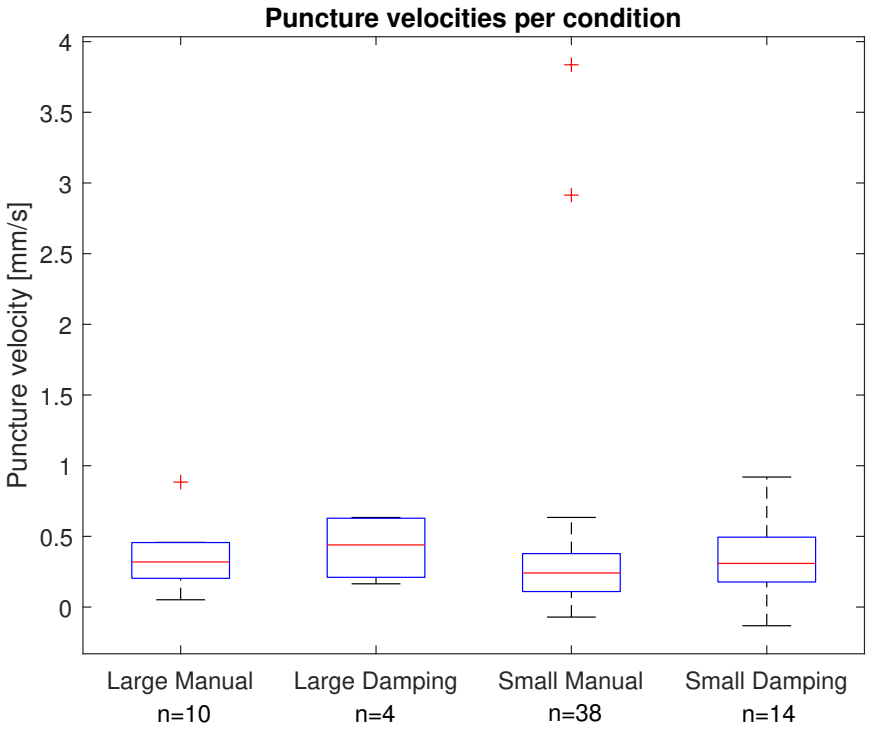

Figure D.1: Boxplot of the puncture velocities per conditions. The total number of punctures per condition is given as well